Check for updates

LIMNOLOGY and OCEANOGRAPHY

ASLO

Limnol. Oceanogr. 66, 2021, 3811–3827
© 2021 Association for the Sciences of Limnology and Oceanography.
doi: 10.1002/lno.11920

Zooglider-measured association of zooplankton with the fine-scale vertical prey field

Benjamin M. Whitmore ,* **Mark D. Ohman**
Scripps Institution of Oceanography, University of California San Diego, La Jolla, California

Abstract

We use *Zooglider*, a low-power optical zooplankton-sensing glider, to test the covariability of the fine-scale vertical distributions of six omnivorous zooplankton taxa with three different representations of their potential prey field: small suspended particles (equivalent circular diameter [ECD] between 0.25 and 0.45 mm), marine snow (ECD ≥ 0.45 mm), and chlorophyll *a* (Chl *a*), in the San Diego Trough. All three prey fields tend to be highly correlated from 100 m to the depth of the subsurface Chl *a* maximum layer (SCML), while correlations between the prey fields are weaker or nonexistent from the SCML to the surface. An index of spatial overlap (Local Index of Collocation) showed stronger overlap of zooplankton with marine snow or small particles than with Chl *a* in most cases. Moreover, generalized additive models revealed marine snow distributions or small particles as the primary explanatory variable, by percent deviance explained, for all zooplankton taxa tested. Chl *a* distributions were a secondary explanatory variable for four of the six taxa tested (small copepods, appendicularia-*Fritillaria*, and both night and day large copepods), and an insignificant explanatory variable for the remaining two (appendicularia-others and large protists). The distributions of suspended particles, during our year-round study in the San Diego Trough, were more informative for explaining distributions of omnivorous zooplankton than Chl *a* alone.

For decades, studies of planktonic trophic interactions have utilized vertical chlorophyll *a* (Chl *a*) distributions as a proxy for the vertical structure of phytoplankton. These distributions are heterogeneous in nature and in most cases exhibit a subsurface Chl *a* maximum layer (SCML) (Cullen 2015). The depth of the SCML is highly variable and is a function of nutrient and light availability, but also grazing pressure (Mullin and Brooks 1976), physiological adaptation (Steele 1964), sinking rate, buoyancy regulation, and swimming behavior (Cullen 2015). Additional physical variables influencing the depth of the SCML are density, nitracline depth (Aksnes et al. 2007), temperature, turbulence, and internal waves (Franks 1995). The depth of the chlorophyll maximum can sometimes correspond to the depth of the phytoplankton biomass maximum (Cullen 1981), but shade adaptation (Chekalyuk and Hafez 2011), and nonphotochemical quenching of fluorescence (Omand et al. 2017) can alter this pattern. In general, Chl *a* distributions are thought to provide insight as to where potential food sources are located, provided it is measured at the scale of interaction for grazers.

In addition to Chl *a*, vertical distributions of suspended detrital particles or organic aggregates (i.e., marine snow) are also frequently measured in the water column. Marine snow ranges in size from sub-millimeters to centimeters, as measured by equivalent circular diameter (ECD). Typically, "large" marine snow is classified as having an ECD greater than 500 μm (Silver et al. 1978). These larger particles are primarily made up of biogenic material, (e.g., planktonic remains, fecal pellets, and molts), but can also contain inorganic components, (e.g., clay aggregates, sediment particles, trace elements, and other compounds [*see* references in Fowler and Knauer 1986]). Due to variable sinking rates, it is possible for layers of higher concentrations of marine snow to form at sharp density transitions (Prairie et al. 2015).

Marine snow aggregations have been found to be variably associated with the SCML. Timmerman et al. (2014) observed a marine snow layer composed of toxic *Pseudo-nitzschia* flocs to be coincident with both the SCML and pycnocline in Monterey Bay. In the highly stratified Northern Gulf of Mexico, Greer et al. (2020) observed using the In situ Ichthyoplankton Imaging System that marine snow aggregates, with ECD > 1.4 mm, were spatially variable in relation to the SCML, with peaks in marine snow concentrations found displaced from or within the SCML. The dominant marine snow shape within the SCML tended to be more round, while marine snow located above and below the SCML was more elongate. This spatial variability

*Correspondence: bmwhitmo@ucsd.edu

Additional Supporting Information may be found in the online version of this article.

was hypothesized to be associated with the different sinking properties of the aggregates.

Layers of marine snow are a potential food source for omnivorous zooplankton whose feeding traits (Litchman et al. 2013; Kiørboe et al. 2018) extend beyond living phytoplankton alone. Based on the evidence that many zooplankton taxa are often associated with marine snow, the broad size range of marine snow, and the presence of fecal pellets, Silver et al. (1978) argued that marine snow could be serving as a food source for zooplankton. Shanks and Walters (1997) observed using SCUBA and vertical flumes that many zooplankton and meiofauna may spend several hours per day residing in or near marine snow aggregates. In the Gulf of Maine, Malkiel et al. (2006) revealed through holography that high densities of copepods were coincident with maximum concentrations of marine snow. Using a video plankton recorder in combination with a Multi-net, Möller et al. (2012) found that distributions of marine snow and copepods were positively correlated in the Baltic Sea. Furthermore, Malkiel et al. (2006), Möller et al. (2012), and Ohman (2019) captured images of copepods appearing to be attached to marine snow. Conversely, copepod abundances in some shelf ecosystems (Stellwagen Bay and the Northern Gulf of Mexico) have been primarily aggregated near the surface, where marine snow abundances were relatively low (Greer et al. 2014, 2020). Moreover, Napp et al. (1988) found in the Southern California Bight that zooplankton biomass composed primarily of copepods coincided with the SCML, but only at night. As copepods have also been shown to be relatively diverse consumers of phytoplankton and ciliates, the copepod association with marine snow could depend on the trophic state of the ecosystem (i.e., the relative concentrations of phytoplankton or ciliates within the water column [Ohman and Runge 1994; Calbet and Saiz 2005]).

Due to high colonization rates of marine snow by copepods, Kiørboe and Thygesen (2001) hypothesized that cruising zooplankton may be able to detect chemical cues from sinking marine snow. This hypothesis was later supported when Lombard et al. (2013) showed that the copepod *Temora longicornis* was capable of detecting, tracking, and attaching to marine snow particles (discarded appendicularian houses) to feed. Incubations have confirmed that hyperiid amphipods (*Themisto compressa*), copepods (*Calanus pacificus*), and euphausiids (*Euphausia pacifica*), among others, all consume marine snow (Lampitt et al. 1993; Dilling et al. 1998). Recent gut content analysis in the Beaufort Sea has revealed that the traditionally considered carnivorous chaetognath *Eukrohnia hamata* could be consuming marine snow and diatoms (Grigor et al. 2020). Euphausiids can both consume marine snow, repackaging it into fecal pellets that sink rapidly out of the euphotic zone, and can fragment large aggregates of marine snow into smaller, slower-sinking particles that have longer residence times in surface waters (Dilling and Alldredge 2000).

Marine snow aggregates have also been shown to fluoresce to some extent.

Briseño-Avena et al. (2020) observed using a planar laser imaging fluorometer in combination with a shadowgraph imaging system (O-Cam) that grazing zooplankton and their predators had night-time vertical distributions that were collocated with or shallower than the SCML and fluorescent particle maximum (FPM) in the Southern California Bight. The large fluorescent particles (i.e., marine snow) that compose the FPM were observed with no coincident peak in bulk Chl *a* fluorescence (Prairie et al. 2010); therefore, these particle distributions would have been missed without the use of imaging systems. It is important to note that even with imaging systems, it is sometimes difficult to discriminate between a concentrated layer of marine snow and a layer of aggregated phytoplankton when they are collocated (Timmerman et al. 2014; Greer et al. 2020).

In contrast to direct feeding on suspended particles, some zooplankton taxa exhibit flux feeding behavior on sinking particles and marine snow. The concept of flux feeding was introduced by Jackson (1993) as an explanation for the existence of particle-consuming zooplankton (e.g., pteropods) in the subeuphotic zone and has since been confirmed by several studies (e.g., Dagg 1993; Stukel et al. 2018). In situ observations from the particle sensing system Sounding Oceanographic Lagrangian Observer and Laser Optical Particle Counter (SOLOPC) showed numerous zooplankton-like particles (i.e., inferred flux feeders) at the base of a particle-rich (marine snow) zone (Jackson and Checkley Jr. 2011). Aulosphaeridae, an abundant family of Phaeodaria in the California Current Ecosystem, were capable of intercepting >20% of sinking particles produced in the euphotic zone before these particles reach 300 m (Stukel et al. 2018). *Limacina helicina* (pteropod) and Aulosphaeridae were found to be responsible for 10%–20% and $\sim$ 10%, respectively, of the total carbon flux attenuation directly below the euphotic zone (Stukel et al. 2019).

Hence, zooplankton can be associated with SCML and marine snow in several ways. At present it is difficult to assess whether suspension-feeding and flux-feeding mesozooplankton are more closely associated with one potential prey source (phytoplankton Chl *a*, small suspended particles, or larger marine snow) in the water column because living phytoplankton and other particles are often co-located vertically (Timmerman et al. 2014). Furthermore, the vertical resolution of conventional zooplankton samplers is insufficient to resolve small differences in vertical offsets of mesozooplankton and their potential prey (Möller et al. 2012). Improved understanding of whether mesozooplankton are preferentially associated with a particular prey source will accelerate our ability to quantify trophic transfer rates (Greer 2013; Greer and Woodson 2016; Briseño-Avena 2015; Briseño-Avena et al. 2020; Greer et al. 2020), the fate of marine snow (Möller et al. 2012; Biard and Ohman 2020), and mesozooplankton survival. Therefore, we pose the question: of potential food sources, are the vertical distributions of suspension-feeding and flux-feeding

mesozooplankton better associated with Chl *a*, small particles (ECD: 0.25–0.45 mm), or marine snow (ECD ≥ 0.45 mm)?

Methods

We address this question using *Zooglider* (Ohman et al. 2018), a fully autonomous mesozooplankton sensing glider, outfitted with a pumped conductivity–temperature–depth (CTD) probe, Chl *a* fluorometer, dual frequency (1000 and 200 kHz) and single beam Zonar, and a low-power telecentric camera (Zoocam) that is capable of resolving vertical distributions of mesozooplankton and marine snow at 5 cm vertical resolution (Gaskell et al. 2019; Ohman 2019; Whitmore et al. 2019). Zoocam utilizes a shadowgraph imaging technique to record images on its onboard camera (FLIR Chameleon), with an approximate imaging volume of 250-mL per frame. *Zooglider* was deployed in the San Diego Trough, approximately 30 km west of La Jolla, California. There were seven 1–2-week deployments from July 2017 to October 2018 (Table 1). Deployments were generally spaced 2–3 months apart. Six of the seven deployments sampled approximately the same region with the mean dive locations separated by < 1 km. The first deployment, July–August 2017, sampled ~ 10 km northeast of the other six deployments and had a shorter deployment duration (7 d compared to 10–14 d). Average water depth for the set of six deployments in proximity and the single offset deployment were > 900 and > 800 m, respectively.

Zooglider conducted eight dives per day, spaced by ~ 3-h intervals, to depths of at least 400 m. Each dive had an average vertical ascent speed of 10 cm s^{-1}, an average ascent angle of ~ 17°, and sampling was conducted solely during ascent. *Zooglider* was equipped with a Seabird CP41 pumped CTD and a Seapoint mini-SCR Chl *a* fluorometer, both of which recorded at 8 s intervals. Chl *a* fluorescence was calibrated against pure extracts of Chl *a* and natural seawater from the pier of the Scripps Institution of Oceanography (Lilly et al. 2019), with an approximate equivalence of 280 counts ≈ 1 μg Chl *a* L^{-1}. However, we report Chl *a* values only in digital count units because of the potential variability in such calibration relationships, as discussed below. *Zooglider* also has a Zonar that samples at 200 and 1000 kHz (but is not considered further here) and a "Zoocam" that acquires ~ 1.2 MB images at 2 Hz. Each image sampled a 250 mL volume at a resolution of 40 μm $pixel^{-1}$. Due to the different sampling frequencies, each CTD measurement was assigned to the frame with the nearest timestamp, and linear interpolation was used to assign CTD measurements to frames that occurred between CTD measurements. For a complete description of *Zooglider* engineering details, *see* Ohman et al. (2018).

Table 1. Deployment summary of manually validated *Zooglider* dives.

Deployment	Day dives	Night dives
Jul–Aug 2017	3	0
Sept 2017	23	16
Nov–Dec 2017	14	21
Jan–Feb 2018	14	25
Apr 2018	21	24
Jul–Aug 2018	26	18
Oct 2018	19	22

Image processing

All images were flat-fielded, segmented, and cropped into specific regions of interest (ROI) following Ohman et al. (2018). If a ROI had an ECD between 0.25 and 0.45 mm, it was enumerated, but not extracted, because we found ROIs of that size comprised too few pixels to assign a meaningful identity and the segmentation process was fine-tuned for larger ROIs (i.e., mesozooplankton). If a ROI had an ECD ≥ 0.45 mm, it was extracted. Occasionally, in the near surface waters (depth < 2 m), the Zoocam became saturated by sunlight and the segmentation algorithm failed to recognize all small ROIs and marine snow. Those saturated frames were highly biased and were removed from the analysis. Each extracted ROI had 70 geometric features calculated and was initially classified using a convolutional neural network (CNN) that leverages contextual metadata to increase classification accuracy (Ellen et al. 2019), into one of 27 categories. All of these categories were manually validated, with the exception of the "marine snow" category due to the number of images. Our machine-learning algorithm was shown to have a ~ 6.6% false-positive rate with respect to wrongly classifying one of the other 26 categories as marine snow (Ellen et al. 2019). This algorithm had a 1% false-positive rate with falsely classifying one of the six zooplankton taxa used in this study as marine snow (Ellen et al. 2019). Thus, these six zooplankton taxa were shown to be robust categories for automated CNN classification. Approximately half of the dives per deployment were manually validated and used for data analysis. Manual validation consisted of analyzing consecutive dives for ~ 5 consecutive days per deployment. Dives were labeled as either day or night depending on comparisons of dive start and end times with nautical twilight. The total number of day and night dives manually validated for each deployment is shown in Table 1.

Six categories of organisms were selected for this study consisting of zooplankton taxa that are primarily suspension-feeding or flux-feeding (Stukel et al. 2019) organisms: appendicularia (*Fritillaria*), appendicularia (others), large protists (including Acantharia, Collodaria, Foraminifera, and Phaeodarea, but strongly dominated by Acantharia), small copepods (feret diameter ≤ 3 mm), large copepods day and night (feret diameter > 3 mm). *Fritillaria* spp. were distinguished from other appendicularia because they are visually distinctive. The 3-mm feret diameter threshold for small and

large copepods was chosen based on significant differences in diel vertical migration (DVM) behavior ($p < 0.001$, t-test). To arrive at the 3-mm feret diameter threshold for copepods, we began by analyzing size classes similar to those used by Ohman and Romagnan (2016). If adjoining size classes showed no significant difference in DVM those size classes were then combined. These six zooplankton categories (*Fritillaria*, appendicularia-others, large protists, small copepods, large copepods day, and large copepods night) consistently had the highest abundances among all deployments, together representing 94.9% ± 3.1% of the total classified zooplankton, and have been shown to be associated with and/or feed upon either phytoplankton or marine snow (Sato et al. 2003; Möller et al. 2012; Stukel et al. 2019).

The potential prey spectrum for grazing/omnivorous zooplankton included small enumerated, but unidentified, ROIs between 0.25 and 0.45 mm (hereafter referred to as small particles), any ROIs identified as marine snow, and Chl *a* fluorescence digital counts. Microzooplankton were most likely included in the counts of marine snow, but they were found through manual validation of the machine learning classifier to be a minor contaminant (< ~ 5% of images). Microzooplankton were also likely included in the small particle counts; however, as the small particles were not identified, we cannot discern their contribution to the small particles category. For marine snow and small particles, it was assumed the observed area of the particle was equivalent to the 2D projection of a sphere; therefore, biovolume estimates were made using the assumption of equivalent spherical volume ($4/3\pi r^3$). The radius, r, for snow biovolume was half the calculated ECD of each ROI labeled as snow, while the radius for the small particles was assumed to be a constant 0.175 mm (half the midpoint value for particles with ECD between 0.25 and 0.45 mm). This assumption, which does not allow for variation in the size of the small particles, was made because no size information was available for the small ROIs, which were not retained during the ROI detection process.

Physical and biological data processing

Deployment mean values of potential density (σ_θ), buoyancy frequency squared (N^2), marine snow, small ROIs, and Chl *a* were used to compare physical and biological properties of the water column across deployments.

Vertical distributions of the numerical (number L^{-1}) or biovolume ($mm^3\ L^{-1}$) concentrations for all categories were corrected for volume of water sampled per image and binned at 0.8 m intervals to correspond to the smallest vertical distance between CTD measurements. All categories were initially dichotomized by day and night to check for diel differences. Significant day–night differences in weighted mean depths ($p < 0.001$, t-test) were observed in both the large and small copepod categories. However, partitioning the small copepods or other zooplankton categories by time of day did not significantly change results of their prey associations. Therefore, small copepods, *Fritillaria*, appendicularia-others, and large protists were each considered as a pooled day + night group, whereas large copepods remained separated by day and night.

The vertical distributions (bin = 0.8 m) of all prey sources and zooplankton taxa were plotted as functions of each of the three prey fields, for all dives within a deployment. Pearson product–moment correlations were then calculated utilizing the entire data set of individual dives within a given deployment to determine the correlations of each prey field with one another. p-Values for all correlations were corrected for multiple testing using the Bonferroni correction.

The depth distribution for the correlation analysis varied by taxon. The depth distributions for small copepods, *Fritillaria*, appendicularia-others, and large protists was 0 to 100 m, as these taxa had greater than 75% of their abundances shallower than 100 m. In contrast, the large copepods were distributed throughout the water column during the day, and shallower at night. Therefore, it was necessary to analyze the large copepods (day and night) distributions from 0 to 400 m to evaluate the potential impact of DVM on the associations of the large copepods with their prey sources.

Local index of collocation as a measure of spatial overlap

To calculate the degree of spatial overlap between our zooplankton taxa and each potential prey source we use the Local Index of Collocation (LIOC). The LIOC overlap index was first developed by Pianka (1973) to study niche overlap in lizards and is commonly used within ecology to estimate the degree of correlation between two density distributions (Carroll et al. 2019). LIOC is calculated using Eq. 1, with P_{pred} and P_{prey} representing the proportions of the total numbers of predators and prey in the same given depth bin. LIOC yields a value of 1 if two populations are in complete overlap and a value of 0 if two populations have complete separation (Carroll et al. 2019).

$$\text{LIOC} = \frac{\sum_i^n \left(P_{\text{pred}_i} * P_{\text{prey}_i}\right)}{\sqrt{\sum_i^n \left(P_{\text{pred}_i}\right)^2 * \sum_i^n \left(P_{\text{prey}_i}\right)^2}}. \quad (1)$$

LIOC values were calculated for all consumer taxa compared to each potential prey source from the surface to 100 m (*Fritillaria*, appendicularia-others, large protists, and small copepods) or 400 m (day and night large copepods) at 0.8-m bin intervals across all dives. Means and 95% confidence intervals from a t-distribution were generated from all of the obtained LIOC values. There were only slight variations in the degree of overlap throughout the year, hence dives from all deployments were combined to form an across-mission overview of the overlap of different zooplankton taxa with potential prey sources.

Generalized additive models

We created generalized additive models (GAMs) to find the best explanatory variable for vertical abundance distributions

of each zooplankton taxon, using R version 3.6.1 (mgcv library, Wood 2017). The abundance of each taxon was estimated as a function of three predictor variables (Chl *a*, marine snow, and small particles). Each predictor variable used a simple spline and "*k*" was set to 5 for all variables to limit overfitting of the sparser data density near the maximum concentrations of each predictor. The best results (greatest deviance explained) were obtained for all taxa by combining all three predictor variables into one model. However, to simplify the model and identify the relative roles of the different prey types on each zooplankton taxon, predictor variables were removed if they improved model performance by less than 5% from the maximum deviance explained using all three predictor variables.

Results

Variations in physical and biological variables across deployments

Potential density (σ_θ) profiles showed a range of mixed layer depths and pycnocline strengths across our study in the San Diego Trough (Fig. 1A). There was a progression of stratification from a shallower mixed layer in the summer (July–August 2017 and 2018), to a better defined, somewhat deeper mixed layer during the winter (January–February 2018) and spring (April 2018). Buoyancy frequency squared (N^2) profiles showed clear differences in the degree of density stratification among the deployments (Fig. 1B). The July–August (2017 and 2018) deployments were the most stratified, while the January–February 2018 and April 2018 deployments were the least stratified. Profiles of in vivo fluorescence of Chl *a* all showed a single SCML and relatively low values of Chl *a* in the near surface waters (Fig. 1C). Conversely, the maxima of marine snow (Fig. 1D) and small particles (Fig. 1E) persisted over a much wider depth range and often had the highest concentrations in near-surface waters. To view the full vertical distributions of the physical variables and prey fields down to 400 m, *see* Supporting Information Fig. S1.

Fritillaria and other appendicularian taxa ("appendicularia-others") displayed markedly different vertical distributions, with *Fritillaria* generally showing deeper abundance maxima than appendicularia-others (Fig. 2A,B), apart from July–August 2018. Large protists (dominated by acantharians) usually showed their highest densities from 0 to 50 m, and during summer months (July–August 2017 and 2018) had noticeably higher densities near the surface < 20 m (Fig. 2C). Small copepods (Fig. 2D) and appendicularian-others did not have clearly defined vertical maxima; however, both taxa generally showed

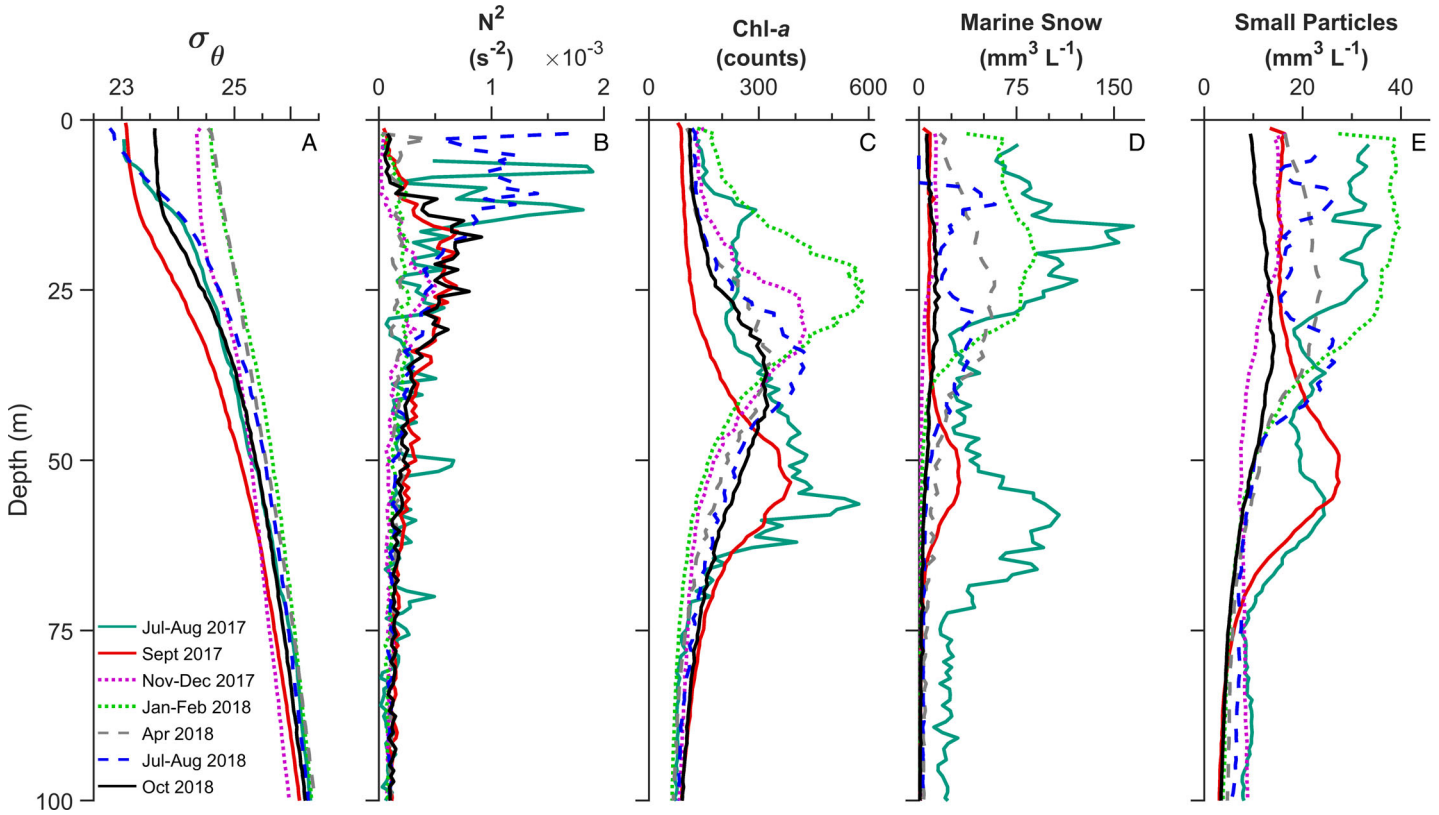

Fig. 1. Summary vertical profiles of water column properties and potential prey sources for all seven *Zooglider* deployments (0–100 m). (**A**) Potential density (σ_θ), (**B**) buoyancy frequency squared (N^2), (**C**) Chl *a* fluorescence, (**D**) marine snow biovolume, and (**E**) small particle biovolume. Each vertical profile represents the mean of all dives (both day and night) within a deployment.

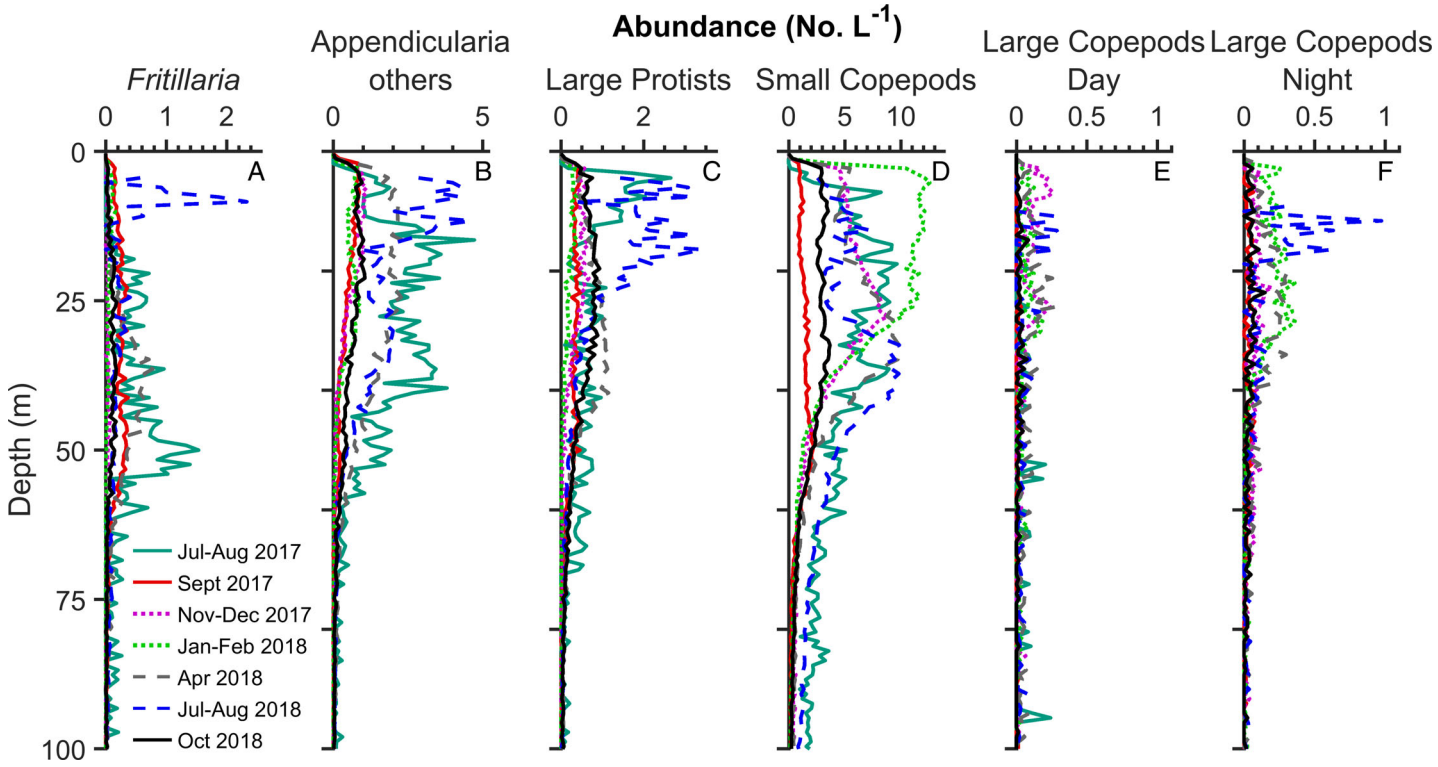

Fig. 2. Summary vertical profiles of mesozooplankton taxa for all seven *Zooglider* deployments (0–100 m). (**A**) *Fritillaria*, (**B**) other appendicularia, (**C**) large protists, (**D**) small copepods (feret diameter ≤ 3 mm), (**E**) large copepods (feret diameter > 3 mm) by day, (**F**) large copepods by night (all as no. L^{-1}). Each vertical profile represents the mean of all dives within a deployment.

their greatest densities in shallower waters. Large copepod abundances increased during the night; however, there was still a portion of large copepods near the surface by day, likely indicating interspecific differences in DVM behavior (Fig. 2E, F). When viewing the mesozooplankton taxa vertical profiles down to 400 m (Supporting Information Fig. S2), it is evident that the majority of the mesozooplankton reside shallower than 100 m for *Fritillaria* (mean of all dives ± SEM: 81% ± 2.9%), appendicularia others (91% ± 2.4%), large protists (83% ± 1.8%), and small copepods (78.7% ± 4.0%). The populations of large copepods were more concentrated shallower than 100 m at night (68% ± 8.2%) compared to the day (39% ± 7.5%). Furthermore, the daytime distributions of large copepods were distributed from 0 to 400 m, while the other taxa were not (Supporting Information Fig. S2).

Covariability of potential prey

We show the extent of covariability among potential prey types (small particles, marine snow, and Chl *a*) for a *Zooglider* deployment in an unstratified condition (January–February 2018, Fig. 3A–C) and a stratified condition (July–August 2018, Fig. 3D–F). All of the prey variables had stronger positive cross correlations in deeper waters (100 m to the SCML, r_{deep}) compared to shallower waters (SCML to the surface, $r_{shallow}$), regardless of the degree of stratification. However, there was greater difference in the strengths of the correlations during unstratified conditions ($r_{shallow}$: 0.33–0.42; r_{deep}: 0.79–0.90) compared to stratified conditions ($r_{shallow}$: 0.37–0.53; r_{deep}: 0.56–0.65). From the SCML to the surface, the relationships between prey variables were substantially weaker than the relationships seen in deeper water ($p < 0.001$). In near-surface waters, in January–February, there was little variation in small particles or marine snow over a broader range of values of Chl *a* (Fig. 3A,B). In the stratified season (Fig. 3D–F), marine snow and small particles first decreased with increasing Chl *a* (Chl *a* counts of 100–180 and depths of 12.2–24.8 m) then increased with increasing Chl *a* (Chl *a* counts of 200–400 and depths of 22.8–34.8 m). Measures of prey covariability (Pearson's correlation with Bonferroni-corrected alpha levels) for all *Zooglider* deployments may be found in Table S1. The majority of deployments, with the exception of November–December 2017, showed the prey fields to be consistently better correlated at depth compared to shallower waters.

Covariability of zooplankton taxa with potential prey

We show the associations of zooplankton consumers with potential prey for an unstratified deployment (Fig. 4) and stratified deployment (Fig. 5). Regardless of stratification level, the abundance of the appendicularian *Fritillaria* showed weak positive relationships with all three potential prey at depth

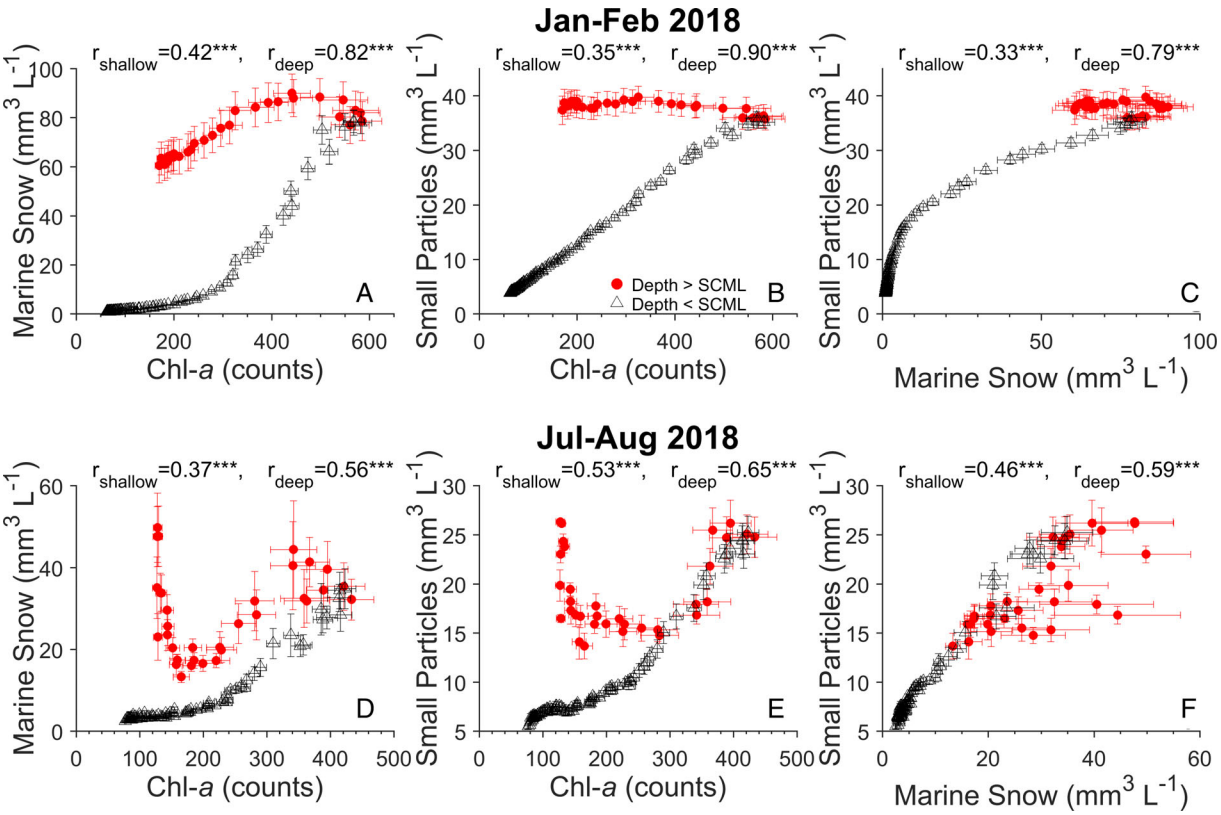

Fig. 3. Associations of the three different potential prey types (Chl *a*, marine snow, small particles) with one another during (**A**–**C**) a low stratification deployment (January–February 2018) and (**D**–**F**) a highly stratified deployment (July–August 2018). Filled red circles represent data between the depth of the Chl *a* maximum (SCML) and the surface, while open black triangles denote data between the SCML and 100 m. Each marker denotes the mean of all dive data in a deployment for a given depth bin, while the error bars represent the 95% confidence intervals for the given depth bin. Pearson correlations for the open black triangles and filled red circles are r_{deep} and $r_{shallow}$, respectively. Bonferroni-corrected alpha levels of significance are *< 0.05, **< 0.01, ***< 0.001.

(r_{deep}: 0.05–0.23) and negligible-to-weak correlations with prey near the surface, $r_{shallow}$: −0.08 to 0.26, (Figs. 4A–C, 5A–C). Compared to *Fritillaria*, appendicularia-others showed stronger positive correlations with prey at depth, r_{deep}: 0.46–0.68, $p < 0.001$, but similarly weak correlations at the surface, $r_{shallow}$: 0.07–0.36, (Figs. 4D–F, 5D–F). Large protists also showed consistently moderate positive correlations with all prey variables at depth, r_{deep}: 0.34–0.42, $p < 0.001$, and weak negative to weak positive correlations near the surface, $r_{shallow}$: −0.35 to 0.27, (Figs. 4G–I, 5G–I).

Small copepods showed the strongest significant positive relationship, of all tested mesozooplankton taxa, with all potential prey variables in the depth zone from 100 m to the SCML, regardless of the stratification level of the deployment (r_{deep}: 0.40–0.83, $p < 0.001$, black triangles, Figs. 4J–L, 5J–L). However, in near-surface waters, small copepod abundance had more variable correlation with each prey source in both the less stratified conditions (Fig. 4J–L, $r_{shallow}$: 0.22–0.73, $p < 0.001$) and the highly stratified conditions (Fig. 5J–L, $r_{shallow}$: 0.10–0.62). In contrast with small copepods, day large copepod abundances generally showed poorer correlation with all potential prey variables. Daytime large copepod abundance (Figs. 4M–O, 5M–O) had weak to negligible correlation with any potential prey variable regardless of stratification or depth in the water column (r_{deep}: 0.07–0.34, $p < 0.001$; $r_{shallow}$: 0.07–0.29). Night distributions of large copepod abundances correlated better with potential prey sources during unstratified conditions (Fig. 4P–Q, r_{deep}: 0.50–0.60, $p < 0.001$; $r_{shallow}$: 0.24–0.41, $p < 0.001$), compared to stratified conditions (Fig. 5P–Q, r_{deep}: 0.25–0.26, $p < 0.001$; $r_{shallow}$: −0.04 to 0.26).

In the majority of deployments, *Fritillaria*, appendicularia-others, large protists, and small copepods, consistently exhibited stronger correlations with all prey sources at depth compared to the near surface waters (Table S2).

Overlap association of zooplankton with potential prey

Fritillaria (Fig. 6A) and large copepods (day and night) (Fig. 6E,F) showed no significant difference in vertical overlap with the three potential prey sources, and all were relatively low. Overlap was somewhat greater with the large copepods and their potential prey sources at night compared to the day. Appendicularia-others (Fig. 6B) and large protists (Fig. 6C) had

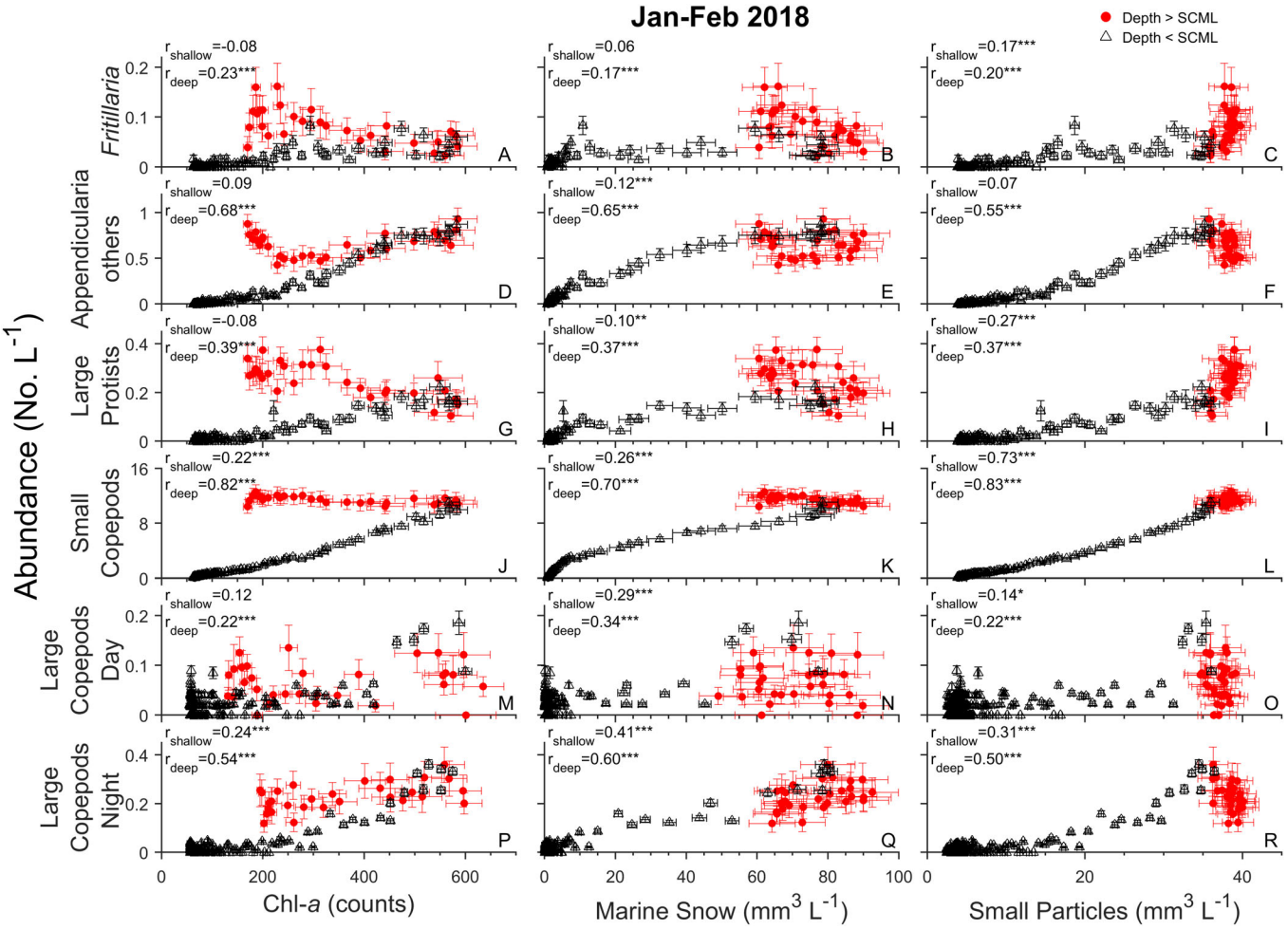

Fig. 4. Low stratification deployment (January–February 2018) in the San Diego Trough. Associations of the three potential prey types (Chl *a*, marine snow, small particles) with abundances of (**A**–**C**) *Fritillaria*, (**D**–**F**) appendicularia others, (**G**–**I**) large protists, (**J**–**L**) small copepods, (**M**–**O**) large copepods (day), and (**P**–**R**) large copepods (night). Filled red circles represent data between the depth of the Chl *a* maximum (SCML) and the surface, while open black triangles denote data between the SCML and 100 m (small copepods) or 400 m (large copepods day and night). Each marker denotes the mean of all dive data in a deployment for a given depth bin, while the error bars represent the 95% confidence intervals for the given depth bin. Pearson correlations for the open black triangles and filled red circles are r_{deep} and $r_{shallow}$, respectively. Bonferroni-corrected alpha levels of significance are *< 0.05, **< 0.01, ***< 0.001.

significantly greater overlap with both marine snow and small particles than with Chl *a*. Small copepods exhibited the greatest spatial overlap with small particles (Fig. 6D). Overall, small copepods showed the greatest overlap with all potential prey among all taxa considered. In contrast, large copepods, both day and night, show the least overlap with these potential preys. *Fritillaria* also showed limited overlap with these potential prey, while appendicularia-others and large protists showed similarly high degrees of overlap with marine snow and small particles.

GAM results

GAM results showed that small copepods had the greatest deviance explained by potential prey sources (52.2%) of any taxon (Table 2). The abundance of small copepods was best explained by small particles, and to a much smaller extent by Chl *a*. Small copepod abundance had a weak linear positive association with Chl *a*, with a potential plateau at higher Chl *a* counts (> 800, Fig. 7A). Small copepods had a positive association with small particle biovolume, with a steeper slope when small ROIs exceed ~ 30 mm^3 L^{-1} (Fig. 7B). Marine snow was found not to be a significant explanatory variable for small copepods.

In contrast to small copepods, the abundance of large copepods showed much less deviance explained in either day (3.9%) or night (21.0%) profiles. The significant prey variables, for large copepods (both day and night) were marine snow and, secondarily Chl *a* (Fig. 7C–F, and Table 2). Marine

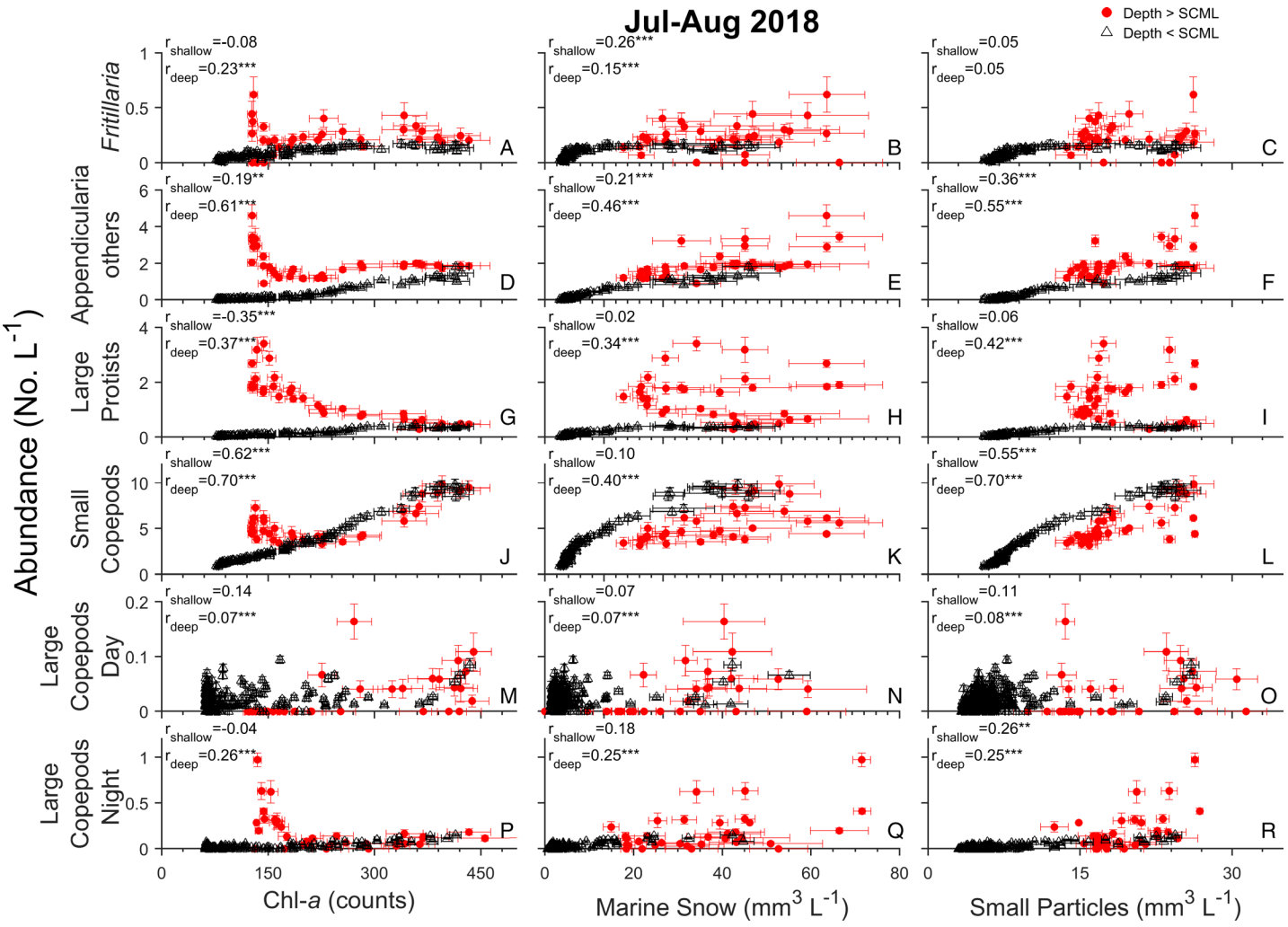

Fig. 5. High stratification deployment (July–August 2018) in the San Diego Trough. Associations of the three potential prey types (Chl *a*, marine snow, small particles) with abundances of (**A**–**C**) *Fritillaria*, (**D**–**F**) appendicularia others, (**G**–**I**) large protists, (**J**–**L**) small copepods, (**M**–**O**) large copepods (day), and (**P**–**R**) large copepods (night). Filled red circles represent data between the depth of the Chl *a* maximum (SCML) and the surface, while open black triangles denote data between the SCML and 100 m (small copepods) or 400 m (large copepods day and night). Each marker denotes the mean of all dive data in a deployment for a given depth bin, while the error bars represent the 95% confidence intervals for the given depth bin. Pearson correlations for the open black triangles and filled red circles are r_{deep} and $r_{shallow}$, respectively. Bonferroni-corrected alpha levels of significance are *< 0.05, **< 0.01, ***< 0.001.

snow concentrations exceeding 150–200 mm^3 L^{-1} were relatively rare, but there was a suggestion of a weakening negative association at such high concentrations (Fig. 7F).

Compared to small and large copepods, both appendicularia-others and *Fritillaria* had intermediate and low levels of deviance explained (32.8% and 13.7%, respectively). Marine snow was the primary predictor variable for both appendicularia categories (*F*-values, Table 2), with both marine snow spline functions showing strong positive linear relationships up to ~ 50 mm^3 L^{-1} (Fig. 8B,D). The remaining significant prey variables for *Fritillaria* were Chl *a* (Fig. 8A) and small particles for both appendicularia others and *Fritillaria* (Fig. 7C,E).

Large protists also showed only intermediate levels of deviance explained (24.9%). There was an increasing positive relationship between marine snow and large protists until concentrations exceeded 50 mm^3 L^{-1} (Fig. 8F). The small particles spline for large protists (Fig. 8G), showed a weaker nonlinear relationship.

Discussion

Zooglider, like other plankton imaging systems (Wiebe and Benfield 2003; Cowen and Guigand 2008; Schulz et al. 2009; Picheral et al. 2010), permits resolution of fine-scale vertical distributions of small suspended particles, marine snow, Chl *a*, and mesozooplankton on the scale at which zooplankton interact with such particles. However, *Zooglider* has the advantage that it is completely autonomous and untethered to a

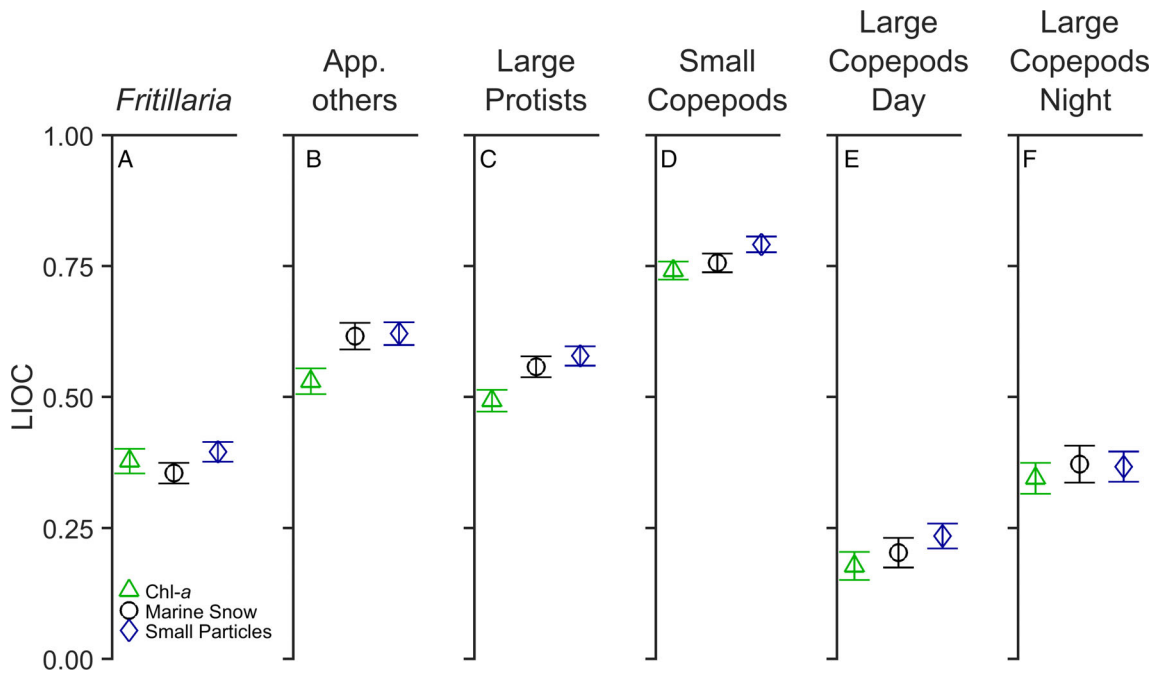

Fig. 6. Local Index of Collocation (LIOC) for all zooplankton taxa and each potential prey type. LIOC = 1 indicates complete overlap, while LIOC = 0 indicates complete separation. Symbols illustrate the mean of all dives from all deployments (± 95% confidence intervals). Panels **A**–**D** from 0 to 100 m; panels **E** and **F** from 0 to 400 m.

Table 2. Deviance in the abundance of different zooplankton taxa explained by significant predictor prey variables, with corresponding *F*-values. Percent difference in deviance explained is the difference between the deviance explained using all three prey predictor variables and the difference explained using only significant variables, divided by the deviance explained using all three prey predictor variables. Insignificant variables resulted in less than a 5% difference in deviance explained when removed.

Taxon	Deviance explained (%)	*F*-value			% Diff. in deviance explained (%)	Depth range
		Chl *a*	Marine snow	Small particles		
Small copepods	52.2	807.8		2402.9	−4.8	0–100 m
App others	32.8		962.9	532.9	−1.0	0–100 m
Fritillaria	13.7	159.0	178.4	160.9		0–100 m
Large protists	24.9		514.6	370.3	−1.2	0–100 m
Large copepods day	3.9	77.8	168.1		−2.2	0–400 m
Large copepods night	21.0	292.4	1206.2		−0.5	0–400 m

The grey shaded rows were to aid in visually breaking up the rows.

surface vessel or fixed platform. *Zooglider* revealed that most suspension-feeding omnivorous zooplankton were more closely associated with marine snow and with small particles rather than with Chl *a* fluorescence in the San Diego Trough. This result provides further evidence supporting previous studies (Herman 1983; Roman et al. 1986; Napp et al. 1988; Ohman and Runge 1994; Calbet and Saiz 2005; Briseño-Avena et al. 2020) that a broader spectrum of prey need to be considered, rather than the conventional focus on fluorescing Chl *a* bearing phytoplankton alone. We now consider this result in relation to our three primary taxa: planktonic copepods, appendicularians, and larger protists.

Copepods

The primary predictor variables for the abundance and vertical location of small copepods and large copepods (night) were small particles and marine snow, respectively. We interpret this result as indicating that surface-dwelling copepods were likely feeding on the small particles (small copepods) and marine snow (large copepods-night) that were associated with the lower Chl *a* levels near the surface. The lower explanatory power for the large copepods suggests that they have a different preferred prey field compared to the small copepods. Alternatively, these larger copepods could be performing foraging sorties, a short bout into food-rich layers followed by a sinking

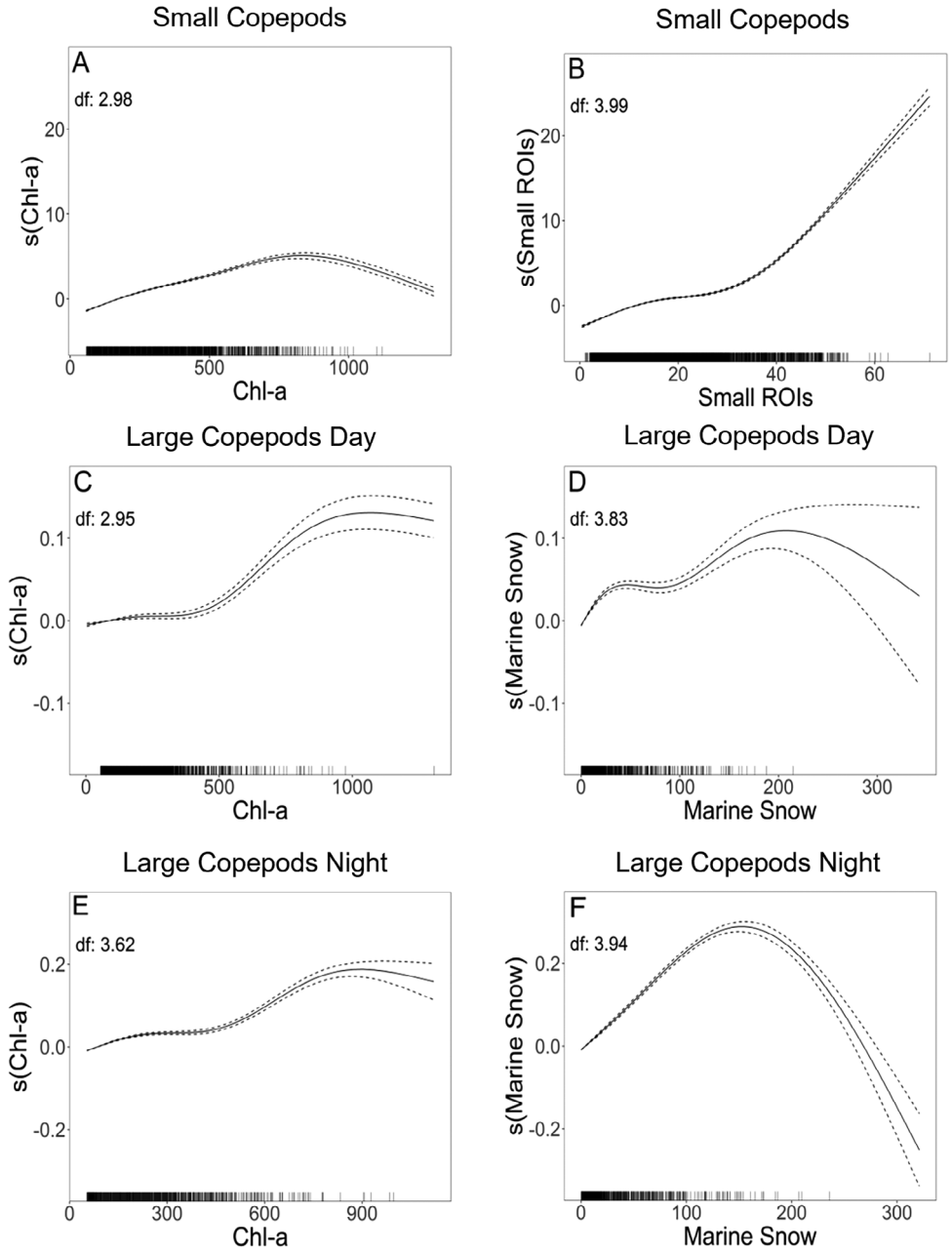

Fig. 7. GAM spline curves of significant prey predictor variables for (**A**,**B**) small copepods, (**C**, **D**) large copepods by day, and (**E**,**F**) large copepods by night. Solid lines represent the mean effect and dashed lines are 95% confidence intervals. The number inside each panel is the effective degrees of freedom of the spline curve. Ticks on the *x*-axis delineate the density of the data used to generate each spline curve. Missing panels indicate that prey variable had an insignificant effect on the total deviance explained.

period while digestion occurs, which would decrease the spatial overlap with their prey when not actively feeding (Karaköylü 2010).

This difference in prey type could also be explained by the difference in diversity of copepod types within the large and small copepod taxa. The large copepods included predatory, omnivorous, and herbivorous copepods, while the smaller copepods were a mix dominated by herbivores and omnivores. The difference in deviance explained between the day and night large copepods was likely attributed to a complex DVM behavior, since daytime vertical distributions of larger, more visually conspicuous copepods were likely more constrained by visual predation risk (e.g., Ohman and Romagnan 2016; Whitmore 2019) than by prey availability.

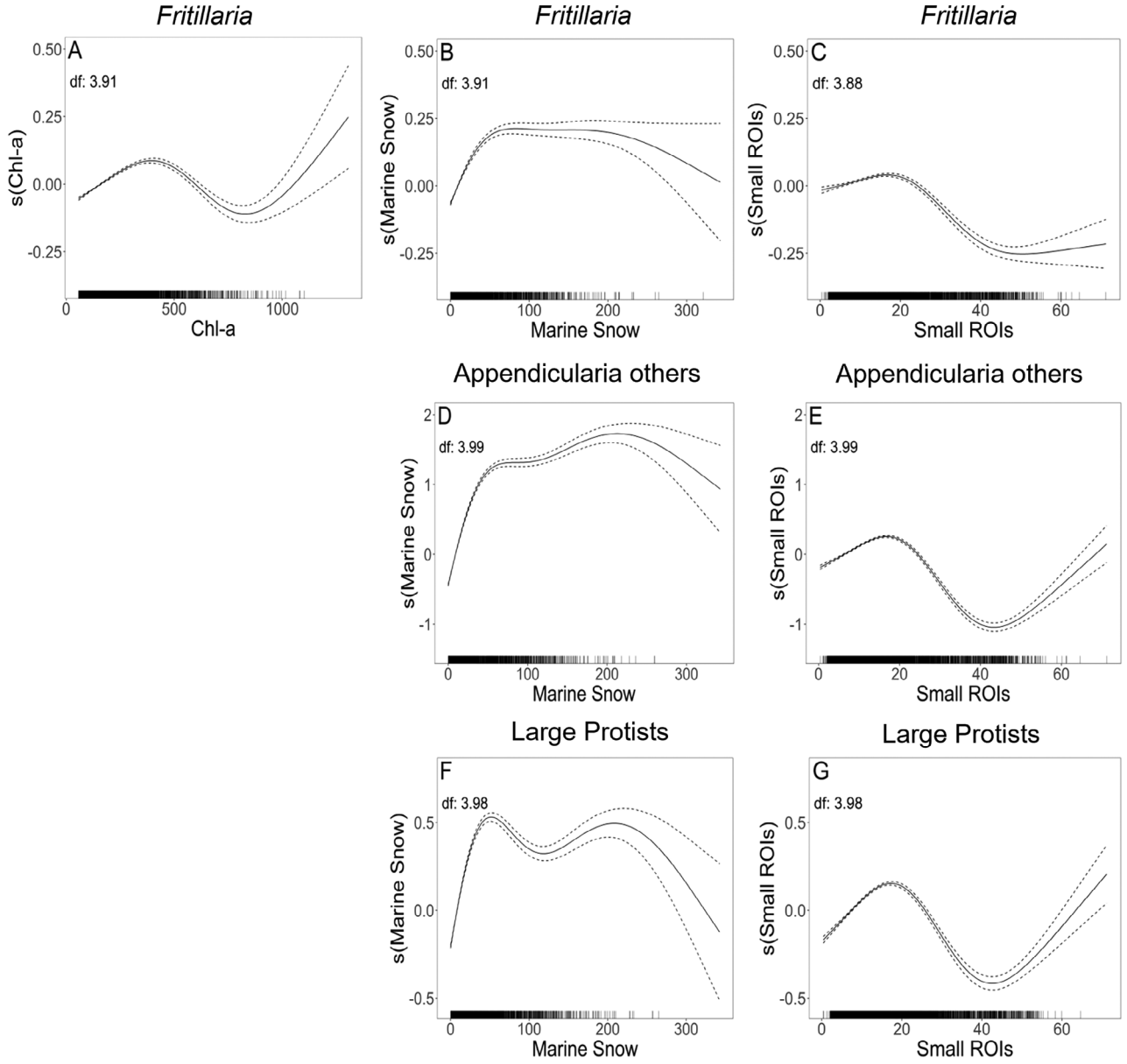

Fig. 8. GAM spline curves of significant prey predictor variables for (**A**–**C**) *Fritillaria*, (**D**,**E**) appendicularia-others, and (**F**,**G**) large protists. Solid lines represent the mean effect and dashed lines are 95% confidence intervals. The number inside each panel is the effective degrees of freedom of the spline curve. Ticks on the *x*-axis delineate the density of the data used to generate each spline curve. Missing panels indicate that prey variable had an insignificant effect on the total deviance explained.

The covariability of copepods with particles has been observed before. Approximately 5% of images of copepods (namely *Pseudocalanus acuspes*) acquired by the Video Plankton Recorder, in the Baltic Sea, showed copepods directly attached to marine snow particles and exhibiting feeding behavior (Möller et al. 2012). Kodama et al. (2018) showed that copepods *Microsetella* spp. and *Oncaea* spp. consumed approximately 13% of discarded appendicularian houses, in the southwestern Sea of Japan. Wilson and Steinberg (2010) showed that copepods feeding on marine snow could enhance the flux of picoplankton to the benthos through fecal pellet production. However, it is important to note that copepods do not always overlap with particle concentrations. Copepods were observed to be primarily located shallower than the FPM and SCML in the Southern California Bight (Briseño-Avena et al. 2020). Conversely, Greer et al. (2020) found copepod

concentrations, in the summer of 2016, to be the highest on the edges of a thin layer of diatoms, in the northern Gulf of Mexico. Moreover, in warm-core Gulf Stream rings, copepods have shown to aggregate in the productivity maximum, which is typically shallower than the SCML (Roman et al. 1986).

Appendicularia

The lower deviance explained by both appendicularian taxa (Appendicularia-others and *Fritillaria*) compared to the small copepods suggests that the potential prey variables we considered may not be as representative of the preferred prey of appendicularia. A portion of this difference may be attributed to the preferred prey size of appendicularia including smaller particles than were directly observable with the Zoocam's image resolution (40 μm pixel^{-1}). Appendicularia obtain ~ 80% of their diets generally from particles with diameters less than 15 μm (*Oikopleura* spp.) and 7 μm (*Fritillaria* spp.) (Fernández et al. 2004), including suspended marine bacteria (King et al. 1980). Some of these smaller (appendicularian prey-sized) particles may be accounted for in the Chl *a* and small particle measurements; however, the overall contribution of these smaller sized particles may be diluted by the presence of larger or more fluorescent particles.

The association of appendicularians with marine snow could be an indicator of elevated abundances of senescent phytoplankton cells that are capable of flocculating to form larger marine snow aggregates. Alternatively, it is possible that the positive association between marine snow and appendicularian abundance is a result of a high number of discarded appendicularian houses co-occurring with the appendicularians themselves. Abandoned appendicularian houses are less likely to co-occur in the water column with the organisms that generated them, due to their high sinking velocities 26–157 m day^{-1} (Gorsky et al. 1984; Hansen et al. 1996). However, these rapidly sinking houses have the potential to settle at sharp density discontinuities (Prairie et al. 2015). Therefore, the fate of these abandoned appendicularian houses could be highly dependent on the stratification of the water column. The discarding of appendicularian houses might also help explain the difference in deviance explained between appendicularia-others and *Fritillaria*. *Fritillaria* spp. renew their houses up to 40 times per day, while appendicularia-others (dominated in our images by *Oikopleura* spp.) have house renewal rates ranging from 2 to 27 houses per day (Sato et al. 2003). The higher house-renewal rate of *Fritillaria* could be necessary to compensate for feeding structures that are more prone to clogging/lower feeding efficiency.

Our observation that appendicularians, other than *Fritillaria*, were more closely associated with marine snow and small particles than with Chl *a* contrasts with previous work that found water column stability and Chl *a* to be the primary environmental factors affecting appendicularian distributions (Capitanio and Esnal 1998; Spinelli et al. 2015). This difference is most likely due to systematic limitations of physical net collections. Net systems are unable to resolve the fine-scale vertical distributions of marine snow and small particles within the water column, while *Zooglider*, like other imaging systems (Wiebe and Benfield 2003; Cowen and Guigand 2008; Schulz et al. 2009; Picheral et al. 2010), is capable of resolving such associations.

Large protists

Large protists showed relatively low levels of deviance explained by marine snow and small particles, with marine snow the primary positive predictor variable. The increasing positive relationship between marine snow and large protists may indicate that large protists utilize marine snow as a food source. Most of the large protists identified in this study (~ 90%–95%) were acantharians. Michaels et al. (1995) also observed acantharians as the numerically dominant large protist in the upper 150 m of the water column. Many acantharians bear photosymbionts (Decelle and Not 2015), and therefore need to reside in the surface waters with greater irradiance. If these photosymbionts provided the dominant component of nutrition for large protists, it could account for the lower deviance explained.

Our results contrast with recent evidence that Chl *a*, the depth of the Chl *a* maximum, and temperature were the best explanatory variables for acantharians ($R^2 = 0.43$, Biard and Ohman 2020, based on Underwater Vision Profiler 5 [UVP5, Picheral et al. 2010] profiles). This difference is most likely attributable to the minimum plankton detection size (600 μm) used in the UVP 5 study; therefore, some of the small acantharians that *Zooglider* (minimum plankton detection size = 450 μm) was able to detect (Whitmore et al. 2019) were likely missed (Biard et al. 2016; Biard and Ohman 2020).

The grazing habits of mineralized protists have been difficult to judge in the past, as net collection often breaks the fragile spines and pseudopodia of many protists (Whitmore et al. 2019; Gaskell et al. 2019). Furthermore, acantharians still intact after net collection dissolve in fixed samples if not supersaturated with strontium chloride (Beers and Stewart 1970). With recent advances in imaging technology, we are starting to observe that mineralized protists account for a larger amount of biomass than previously thought (Biard et al. 2016; Biard and Ohman 2020; Whitmore et al. 2019) and are partitioned into taxon-specific vertical habitats (Biard and Ohman 2020).

Depth-dependence of particle fields

Our results revealed that small particles, marine snow, and Chl *a* have distinctly depth-dependent relationships that differ above and below the SCML. Such pronounced differences illustrate that the same Chl *a* fluorescence measurement can be associated with markedly different concentrations of marine snow or small particles, depending on the depth stratum in the water column. Furthermore, these depth disparities

in concentrations vary by time of year and degree of water-column stratification. Although not unexpected, these results support previous studies (Herman 1983; Roman et al. 1986; Ohman and Runge 1994; Calbet and Saiz 2005; Möller et al. 2012; Briseño-Avena 2015; Briseño-Avena et al. 2020; Greer et al. 2020), showing a distinct limitation of using only Chl *a* as predictors of prey resources to omnivorous zooplankton.

This lack of correspondence between Chl *a* and particle distributions is partly due to three inherent sources of uncertainty associated with in vivo fluorescence. The first is nonphotochemical quenching (NPQ) of Chl *a*, which is known to alter the fluorescence signal per unit Chl *a* on a diel cycle, resulting in a diminution in recorded fluorescence in daylight hours (Omand et al. 2017). However, our previous work with this type of glider-mounted Chl *a* fluorometer has shown that NPQ was most significant in the upper 20–30 m of the water column in southern California waters (Davis et al. 2008). Moreover, extracted Chl *a* and *Zooglider*-measured in vivo fluorescence are highly correlated near our study site in the San Diego Trough (Whitmore et al. 2019) and off Central California (S. Gastauer, pers. comm.). The second source of uncertainty is shade adaptation of phytoplankton (Chekalyuk and Hafez 2011) and the well-known depth-dependence of Carbon : Chl *a* ratios (Taylor et al. 2011). The depth-dependent C : Chl *a* effect will certainly influence our profiles. The third source of uncertainty is the variable species composition and community structure of the phytoplankton, some of which will be solitary picoplankton that are too small to be readily ingested by suspension-feeding crustaceans (Calbet et al. 2000) and others of which will be large (chain lengths > 14 mm) and/or spiny chains that are essentially unavailable as prey to most zooplankton (Ohman 2019).

The uncertainties associated with in situ measured in vivo fluorescence can explain some of the different relationships observed between Chl *a* and particle distributions at different water column stabilities. For instance, in the less-stratified winter deployment, the near-surface small particle abundances were independent of Chl *a*. As mixing can enhance nutrient flow to diatoms and other nonmotile phytoplankton (Barton et al. 2014), this lack of dependence on Chl *a* was likely due to lower Chl *a* concentrations per unit C (Falkowski and LaRoche 1991). Lower surface Chl *a* values with similar concentrations of small particles would be consistent with decreasing C : Chl *a* with greater depth (i.e., decreasing light levels, Taylor et al. 2011). In contrast, the quadratic relationship of small particle concentrations to Chl *a*, observed in July–August 2018, is likely attributable to nutrient limitation. Nutrient limitation ultimately results in the surface-dwelling phytoplankton becoming senescent and sinking rapidly out of the water column (Smayda and Boleyn 1966).

The relationship between marine snow/small particles and Chl *a* is further complicated by the fact that potential prey sources are not independent. The true identity of the small particles (e.g., detritus, microzooplankton, mixotrophs, phytoplankton) cannot be determined with the current Zoocam image resolution (40 μm pixel^{-1}), so we cannot assess the extent of overlap between Chl *a* and small particle distributions, although we assume there is some coincidence. The marine snow category could also be contributing to Chl *a* measurements caused by undigested phytoplankton, fecal pellets, discarded appendicularian houses, or other organic matter (Prairie et al. 2010; Briseño-Avena et al. 2020; Markussen et al. 2020). In addition, some recognizable diatoms could occasionally have been incorrectly classified as marine snow. However, our Machine Learning classifier has a false positive rate of 5%, that is, of falsely labeling recognizable diatoms as snow (Ellen et al. 2019), so this is unlikely to be a significant source of uncertainty.

Conclusions

With the aid of *Zooglider*, we were able to resolve fine-scale vertical distributions of different types of suspension-feeding zooplankton in the San Diego Trough, concurrently with their spatial overlap with different sources of potential prey: Chl *a*, marine snow, and small particles. Using data from seven *Zooglider* deployments spanning July 2017–October 2018, we found that none of the mesozooplankton taxa were strongly associated with Chl *a*, which is the most common metric utilized for mesozooplankton food concentrations. The abundance and vertical distribution of small copepods were best explained by the biovolume of small particles. *Fritillaria*, other appendicularians, and larger mineralized protists were best explained by marine snow and small particles. Large copepods, which generally exhibited DVM behavior, showed deep daytime depths that were best accounted for by predator avoidance behavior and nighttime depths that better coincided with the depths of marine snow. For all mesozooplankton taxa, marine snow or small particles were the primary explanatory variables, rather than Chl *a*.

References

Aksnes, D. L., M. D. Ohman, and P. Rivière. 2007. Optical effect on the nitracline in a coastal upwelling area. Limnol. Oceanogr. **52**: 1179–1187. doi:10.4319/lo.2007.52.3.1179

Barton, A. D., B. A. Ward, R. G. Williams, and M. J. Follows. 2014. The impact of fine-scale turbulence on phytoplankton community structure. Limnol. Oceanogr. Fluids Environ. **4**: 34–49.

Beers, J. R., and G. L. Stewart. 1970. The preservation of acantharians in fixed plankton samples. Limnol. Oceanogr. **15**: 825–827. doi:10.4319/lo.1970.15.5.0825

Biard, T., and others. 2016. In situ imaging reveals the biomass of giant protists in the global ocean. Nature **532**: 504–507. doi:10.1038/nature17652

Biard, T., and M. D. Ohman. 2020. Vertical niche definition of test-bearing protists (Rhizaria) into the twilight zone revealed by in situ imaging. Limnol. Oceanogr. **65**: 2583–2602. doi:10.1002/lno.11472

Briseño-Avena, C. 2015. Fine-scale spatial and temporal plankton distributions in the Southern California Bight: lessons from in situ microscopes and broadband echosounders. Ph. D. thesis. UC San Diego.

Briseño-Avena, C., J. C. Prairie, P. J. Franks, and J. S. Jaffe. 2020. Comparing vertical distributions of Chl-*a* fluorescence, marine snow, and taxon-specific zooplankton in relation to density using high-resolution optical measurements. Front. Mar. Sci. **7**: 1–15.

Calbet, A., M. R. Landry, and R. D. Scheinberg. 2000. Copepod grazing in a subtropical bay: Species-specific responses to a midsummer increase in nanoplankton standing stock. Mar. Ecol. Prog. Ser. **193**: 75–84. doi:10.3354/meps193075

Calbet, A., and E. Saiz. 2005. The ciliate-copepod link in marine ecosystems. Aquat. Microb. Ecol. **38**: 157–167. doi:10.3354/ame038157

Capitanio, F. L., and G. B. Esnal. 1998. Vertical distribution of maturity stages of *Oikopleura dioica* (Tunicata, Appendicularia) in the frontal system off Valdés Peninsula. Argentina. Bull. Mar. Sci. **63**: 531–539.

Carroll, G., and others. 2019. A review of methods for quantifying spatial predator–prey overlap. Glob. Ecol. Biogeogr. **28**: 1561–1577.

Chekalyuk, A., and M. Hafez. 2011. Photo-physiological variability in phytoplankton chlorophyll fluorescence and assessment of chlorophyll concentration. Opt. Express **19**: 22643–22658. doi:10.1364/OE.19.022643

Cowen, R. K., and C. M. Guigand. 2008. *In situ* ichthyoplankton imaging system (*IS*IIS): System design and preliminary results. Limnol. Oceanogr. Methods **6**: 126–132.

Cullen, J. J. 1981. Chlorophyll maximum layers of the Southern Californian Bight and possible mechanisms of their formation and maintenance. Oceanol. Acta **4**: 23–31.

Cullen, J. J. 2015. Subsurface chlorophyll maximum layers: Enduring enigma or mystery solved? Ann. Rev. Mar. Sci. **7**: 207–239. doi:10.1146/annurev-marine-010213-135111

Dagg, M. 1993. Sinking particles as a possible source of nutrition for the large calanoid copepod *Neocalanus cristatus* in the sub-Arctic Pacific Ocean. Deep-Sea Res. I Oceanogr. Res. Pap. **40**: 1431–1445. doi:10.1016/0967-0637(93)90121-i

Davis, R. E., M. D. Ohman, D. L. Rudnick, and J. T. Sherman. 2008. Glider surveillance of physics and biology in the Southern California Current System. Limnol. Oceanogr. **53**part 2): 2151-2168, 5part2.

Decelle, J., and F. Not. 2015. Acantharia, p. 1–10. *In* eLS. John Wiley & Sons, Ltd. doi:10.1002/9780470015902.a0002102.pub2

Dilling, L., J. Wilson, D. Steinberg, and A. Alldredge. 1998. Feeding by the euphausiid *Euphausia pacifica* and the copepod *Calanus pacificus* on marine snow. Mar. Ecol. Prog. Ser. **170**: 189–201. doi:10.3354/meps170189

Dilling, L., and A. L. Alldredge. 2000. Fragmentation of marine snow by swimming macrozooplankton: A new process impacting carbon cycling in the sea. Deep-Sea Res. I Oceanogr. Res. Pap. **47**: 1227–1245. doi:10.1016/S0967-0637(99)00105-3

Ellen, J. S., C. A. Graff, and M. D. Ohman. 2019. Improving plankton image classification using context metadata. Limnol. Oceanogr. Methods **17**: 439–461.

Falkowski, P. G., and J. LaRoche. 1991. Acclimation to spectral irradiance in algae. J. Phycol. **27**: 8–14. doi:10.1111/j.0022-3646.1991.00008.x

Fernández, D., A. López-Urrutia, A. Fernández, J. L. Acuña, and R. Harris. 2004. Retention efficiency of 0.2 to 6 μm particles by the appendicularians *Oikopleura dioica* and *Fritillaria borealis*. Mar. Ecol. Prog. Ser. **266**: 9–101.

Fowler, S. W., and G. A. Knauer. 1986. Role of large particles in the transport of elements and organic compounds through the oceanic water column. Prog. Oceanogr. **16**: 147–194. doi:10.1016/0079-6611(86)90032-7

Franks, P. J. 1995. Thin layers of phytoplankton: A model of formation by near-inertial wave shear. Deep-Sea Res. I Oceanogr. Res. Pap. **42**: 75–91. doi:10.1016/0967-0637(94)00028-Q

Gaskell, D. E., M. D. Ohman, and P. M. Hull. 2019. *Zooglider*-based measurements of planktonic foraminifera in the California Current System. J. Foramin. Res. **49**: 390–404. doi:10.2113/gsjfr.49.4.390

Gorsky, G., N. S. Fisher, and S. W. Fowler. 1984. Biogenic debris from the pelagic tunicate, *Oikopleura dioica*, and its role in the vertical transport of a transuranium element. Estuar. Coast. Shelf Sci. **18**: 13–23. doi:10.1016/0272-7714(84)90003-9

Greer, A. T. 2013. Fine-scale distributions of plankton and larval fishes: Implications for predator-prey interactions near coastal oceanographic features. Ph.D. thesis. Univ. of Miami.

Greer, A. T., R. K. Cowen, C. M. Guigand, J. A. Hare, and D. Tang. 2014. The role of internal waves in larval fish interactions with potential predators and prey. Prog. Oceanogr. **27**: 47–61.

Greer, A. T., and C. B. Woodson. 2016. Application of a predator–prey overlap metric to determine the impact of sub-grid scale feeding dynamics on ecosystem productivity. ICES J. Mar. Sci. **73**: 1051–1061. doi:10.1093/icesjms/fsw001

Greer, A. T., and others. 2020. Contrasting fine-scale distributional patterns of zooplankton driven by the formation of a diatom-dominated thin layer. Limnol. Oceanogr. **65**: 2236–2258. doi:10.1002/lno.11450

Grigor, J. J., and others. 2020. Non-carnivorous feeding in Arctic chaetognaths. Prog. Oceanogr. **186**: 102388. doi:10.1016/j.pocean.2020.102388

Hansen, J. L., T. Kiørboe, and A. L. Alldredge. 1996. Marine snow derived from abandoned larvacean houses: Sinking rates, particle content and mechanisms of aggregate formation. Mar. Ecol. Prog. Ser. **141**: 205–215. doi:10.3354/meps141205

Herman, A. W. 1983. Vertical distribution patterns of copepods, chlorophyll, and production in northeastern Baffin Bay. Limnol. Oceanogr. **28**: 709–719. doi:10.4319/lo.1983.28.4.0709

Jackson, G. A. 1993. Flux feeding as a mechanism for zooplankton grazing and its implications for vertical particulate flux. Limnol. Oceanogr. **38**: 1328–1331. doi:10.4319/lo.1993.38.6.1328

Jackson, G. A., and D. M. Checkley Jr. 2011. Particle size distributions in the upper 100 m water column and their implications for animal feeding in the plankton. Deep-Sea Res. I Oceanogr. Res. Pap. **58**: 283–297. doi:10.1016/j.dsr.2010.12.008

Karaköylü, E. M. 2010. The foraging sorties hypothesis: evaluating the effect of gut dynamics on copepod foraging behavior. Ph.D. thesis. UC San Diego.

King, K. R., J. T. Hollibaugh, and F. Azam. 1980. Predator-prey interactions between the larvacean *Oikopleura dioica* and bacterioplankton in enclosed water columns. Mar. Biol. **56**: 49–57. doi:10.1007/BF00390593

Kiørboe, T., and U. H. Thygesen. 2001. Fluid motion and solute distribution around sinking aggregates. II. Implications for remote detection by colonizing zooplankters. Mar. Ecol. Prog. Ser. **211**: 15–25. doi:10.3354/meps211015

Kiørboe, T., A. P. Visser, and K. H. Andersen. 2018. A trait-based approach to ocean ecology. ICES J. Mar. Sci. **75**: 1849–1863. doi:10.1093/icesjms/fsy090

Kodama, T., N. Iguchi, M. Tomita, H. Morimoto, T. Ota, and S. Ohshimo. 2018. Appendicularians in the southwestern sea of Japan during the summer: Abundance and role as secondary producers. J. Plankton Res. **40**: 269–283. doi:10.1093/plankt/fby015

Lampitt, R. S., K. F. Wishner, C. M. Turley, and M. V. Angel. 1993. Marine snow studies in the Northeast Atlantic Ocean: Distribution, composition and role as a food source for migrating plankton. Mar. Biol. **116**: 689–702. doi:10.1007/BF00355486

Lilly, L. E., U. Send, M. Lankhorst, T. R. Martz, and M. D. Ohman. 2019. Biogeochemical anomalies at two Southern California Current System moorings during the 2014–16 Warm Anomaly-El Niño sequence. J. Geophys. Res. Oceans **124**: 6886–6903. doi:10.1029/2019JC015255

Litchman, E., M. D. Ohman, and T. Kiørboe. 2013. Trait-based approaches to zooplankton communities. J. Plankton Res. **35**: 473–484. doi:10.1093/plankt/fbt019

Lombard, F., M. Koski, and T. Kiørboe. 2013. Copepods use chemical trails to find sinking marine snow aggregates. Limnol. Oceanogr. **58**: 185–192. doi:10.4319/lo.2013.58.1.0185

Malkiel, E., J. N. Abras, E. A. Widder, and J. Katz. 2006. On the spatial distribution and nearest neighbor distance between particles in the water column determined from in situ holographic measurements. J. Plankton Res. **28**: 149–170. doi:10.1093/plankt/fbi107

Markussen, T. N., C. Konrad, C. Waldmann, M. Becker, G. Fischer, and M. H. Iversen. 2020. Tracks in the snow–advantage of combining optical methods to characterize marine particles and aggregates. Front. Mar. Sci. **7**: 1–12.

Michaels, A. F., D. A. Caron, N. R. Swanberg, F. A. Howse, and C. M. Michaels. 1995. Planktonic sarcodines (Acantharia, Radiolaria, Foraminifera) in surface waters near Bermuda: Abundance, biomass and vertical flux. J. Plankton Res. **17**: 131–163. doi:10.1093/plankt/17.1.131

Möller, K. O., M. S. John, A. Temming, J. Floeter, A. F. Sell, J. P. Herrmann, and C. Möllmann. 2012. Marine snow, zooplankton and thin layers: Indications of a trophic link from small-scale sampling with the Video Plankton Recorder. Mar. Ecol. Prog. Ser. **468**: 57–69. doi:10.3354/meps09984

Mullin, M. M., and E. R. Brooks. 1976. Some consequences of distributional heterogeneity of phytoplankton and zooplankton. Limnol. Oceanogr. **21**: 784–796. doi:10.4319/lo.1976.21.6.0784

Napp, J. M., E. R. Brooks, P. Matrai, and M. M. Mullin. 1988. Vertical distribution of marine particles and grazers. II. Relation of grazer distribution to food quality and quantity. Mar. Ecol. Prog. Ser. **50**: 59–72. doi:10.3354/meps050059

Ohman, M. D., and J. A. Runge. 1994. Sustained fecundity when phytoplankton resources are in short supply: Omnivory by *Calanus finmarchicus* in the Gulf of St. Lawrence. Limnol. Oceanogr. **39**: 21–36. doi:10.4319/lo.1994.39.1.0021

Ohman, M. D., and J. B. Romagnan. 2016. Nonlinear effects of body size and optical attenuation on diel vertical migration by zooplankton. Limnol. Oceanogr. **61**: 765–770. doi:10.1002/lno.10251

Ohman, M. D., R. E. Davis, J. T. Sherman, K. R. Grindley, B. M. Whitmore, C. F. Nickels, and J. S. Ellen. 2018. *Zooglider*: An autonomous vehicle for optical and acoustic sensing of zooplankton. Limnol. Oceanogr. Methods **17**: 69–86. doi:10.1002/lom3.10301

Ohman, M. D. 2019. A sea of tentacles: Optically discernible traits resolved from planktonic organisms in situ. ICES J. Mar. Sci. **76**: 1959–1972. doi:10.1093/icesjms/fsz184

Omand, M. M., I. Cetinić, and A. J. Lucas. 2017. Using bio-optics to reveal phytoplankton physiology from a Wirewalker autonomous platform. Oceanography **30**: 128–131. doi:10.5670/oceanog.2017.233

Pianka, E. R. 1973. The structure of lizard communities. Annu. Rev. Ecol. Syst. **4**: 53–74. doi:10.1146/annurev.es.04.110173.000413

Picheral, M., L. Guidi, L. Stemmann, D. M. Karl, G. Iddaoud, and G. Gorsky. 2010. The Underwater Vision Profiler 5: An

advanced instrument for high spatial resolution studies of particle size spectra and zooplankton. Limnol. Oceanogr. Methods **8**: 462–473.

Prairie, J. C., P. J. Franks, and J. S. Jaffe. 2010. Cryptic peaks: Invisible vertical structure in fluorescent particles revealed using a planar laser imaging fluorometer. Limnol. Oceanogr. **55**: 1943–1958. doi:10.4319/lo.2010.55.5.1943

Prairie, J. C., K. Ziervogel, R. Camassa, R. M. McLaughlin, B. L. White, C. Dewald, and C. Arnosti. 2015. Delayed settling of marine snow: Effects of density gradient and particle properties and implications for carbon cycling. Mar. Chem. **175**: 28–38. doi:10.1016/j.marchem.2015.04.006

Roman, M. R., C. S. Yentsch, A. L. Gauzens, and D. A. Phinney. 1986. Grazer control of the fine-scale distribution of phytoplankton in warm-core Gulf Stream rings. J. Mar. Res. **44**: 795–813. doi:10.1357/002224086788401657

Sato, R., Y. Tanaka, and T. Ishimaru. 2003. Species-specific house productivity of appendicularians. Mar. Ecol. Prog. Ser. **259**: 163–172. doi:10.3354/meps259163

Schulz, J., and others. 2009. Lightframe on-sight key species investigation (LOKI), p. 1–5. *In* OCEANS 2009-Europe. IEEE, Bremen, Germany.

Shanks, A. L., and K. Walters. 1997. Holoplankton, meroplankton, and meiofauna associated with marine snow. Mar. Ecol. Prog. Ser. **156**: 75–86. doi:10.3354/meps156075

Silver, M. W., A. L. Shanks, and J. D. Trent. 1978. Marine snow: Microplankton habitat and source of small-scale patchiness in pelagic populations. Science **201**: 371–373. doi:10.1126/science.201.4353.371

Smayda, T. J., and B. J. Boleyn. 1966. Experimental observations on the flotation of marine diatoms. II. *Skeletonema costatum* and *Rhizosolenia setigera*. Limnol. Oceanogr. **11**: 18–34. doi:10.4319/lo.1966.11.1.0018

Spinelli, M., C. Derisio, P. Martos, M. Pájaro, G. Esnal, H. Mianzán, and F. Capitanio. 2015. Diel vertical distribution of the larvacean *Oikopleura dioica* in a North Patagonian tidal frontal system (42°–45° S) of the SW Atlantic Ocean. Mar. Biol. Res. **11**: 633–643. doi:10.1080/17451000.2014.978338

Steele, J. 1964. A study of production in the Gulf of Mexico. J. Mar. Res. **22**: 211–222.

Stukel, M. R., T. Biard, J. Krause, and M. D. Ohman. 2018. Large Phaeodaria in the twilight zone: Their role in the carbon cycle. Limnol. Oceanogr. **63**: 2579–2594. doi:10.1002/lno.10961

Stukel, M. R., M. D. Ohman, T. B. Kelly, and T. Biard. 2019. The roles of suspension-feeding and flux-feeding zooplankton as gatekeepers of particle flux into the mesopelagic ocean in the Northeast Pacific. Front. Mar. Sci. **6**: 397. doi:10.3389/fmars.2019.00397

Taylor, A. G., M. R. Landry, K. E. Selph, and E. J. Yang. 2011. Biomass, size structure and depth distributions of the microbial community in the eastern equatorial Pacific. Deep-Sea Res. II Top. Stud. Oceanogr. **58**: 342–357. doi:10.1016/j.dsr2.2010.08.017

Timmerman, A. H., M. A. McManus, O. M. Cheriton, R. K. Cowen, A. T. Greer, R. M. Kudela, K. Ruttenberg, and J. Sevadjian. 2014. Hidden thin layers of toxic diatoms in a coastal bay. Deep-Sea Res. II Top. Stud. Oceanogr. **101**: 129–140. doi:10.1016/j.dsr2.2013.05.030

Wiebe, P. H., and M. C. Benfield. 2003. From the Hensen net toward four-dimensional biological oceanography. Prog. Oceanogr. **56**: 7–136. doi:10.1016/S0079-6611(02)00140-4

Whitmore, B. M. 2019. *Zooglider* reveals the importance of marine snow, small particles, and body size to planktonic trophic interactions. Ph.D. thesis. UC San Diego.

Whitmore, B. M., C. F. Nickels, and M. D. Ohman. 2019. A comparison between *Zooglider* and shipboard net and acoustic mesozooplankton sensing systems. J. Plankton Res. **41**: 521–533. doi:10.1093/plankt/fbz033

Wilson, S. E., and D. K. Steinberg. 2010. Autotrophic picoplankton in mesozooplankton guts: Evidence of aggregate feeding in the mesopelagic zone and export of small phytoplankton. Mar. Ecol. Prog. Ser. **412**: 11–27. doi:10.3354/meps08648

Wood, S. 2017. Generalized Additive Models: An Introduction with R, 2nd ed. Chapman and Hall/CRC.

Acknowledgments

This work could not have been done without the help of the following individuals: E. Tovar and L. Sala for organism identification; S. Gastauer for implementation and help with the GAM modeling; J. Ellen for the machine learning classification of images and paper edits; S. Matthews for help with editing. We also thank the entirety of the Instrument Development Group at the Scripps Institution of Oceanography for the construction and operation of *Zooglider*. The Gordon and Betty Moore Foundation (grants to M.D. Ohman) supported the development and use of *Zooglider*. The NSF provided financial support for the CCE-LTER program, of which this is a part. BMW was supported by an NSF GRFP and a DoD SMART Scholarship.

Conflict of Interest

None declared.

Submitted 04 August 2020
Revised 07 March 2021
Accepted 05 August 2021

Associate editor: Heidi Sosik

Supporting Information for:

Whitmore, B.W. and M.D. Ohman. 2021. *Zooglider*-measured association of zooplankton with the fine-scale vertical prey field. Limnology and Oceanography 66:3811-3827. doi 10.1002/lno.11920

Supplementary Table 1:

Pearson product-moment correlations of three different potential prey types (Chl-*a*, marine snow, small particles) with one another for all seven *Zooglider* deployments in the San Diego Trough. r_{deep} includes data from 100 m to the depth of the Chl-*a* maximum (SCML). $r_{shallow}$ includes data from the SCML to the surface. Bonferroni-corrected alpha levels: *<0.05, **<0.01, ***<0.001.

	Chl-*a* vs Marine Snow		**Chl-a vs Small Particles**		**Marine Snow vs Small Particles**	
Deployment	r_{deep}	$r_{shallow}$	r_{deep}	$r_{shallow}$	r_{deep}	$r_{shallow}$
Jul-Aug 2017	0.73***	-0.15	0.83***	-0.42***	0.90***	0.79***
Sep 2017	0.85***	0.72***	0.95***	0.81***	0.77***	0.86***
Nov-Dec 2017	0.52***	-0.01	0.20***	0.10*	0.48***	0.83***
Jan-Feb 2018	0.82***	0.42***	0.90***	0.35***	0.79***	0.33***
Apr 2018	0.62***	0.07*	0.88***	0.11***	0.78***	0.78***
Jul-Aug 2018	0.56***	0.37***	0.65***	0.53***	0.59***	0.46***
Oct 2018	0.65***	0.35***	0.90***	0.65***	0.72***	0.73***

Supplementary Table 2: Pearson product-moment correlations of each zooplankton taxon with each of the three different potential prey types (Chl-*a*, marine snow, small particles) for all seven *Zooglider* deployments in the San Diego Trough. r_{deep} includes data from 100 m to the depth of the Chl-*a* maximum (SCML). $r_{shallow}$ includes data from the SCML to the surface. Bonferroni-corrected alpha levels: *<0.05, **<0.01, ***<0.001.

		Chl-*a*		**Marine Snow**		**Small Particles**	
Deployment		**r_{deep}**	**$r_{shallow}$**	**r_{deep}**	**$r_{shallow}$**	**r_{deep}**	**$r_{shallow}$**
l-Aug 2017	Fritillaria	0.28**	0.45***	0.33***	-0.16	0.42***	-0.22*
	App. Others	0.52***	-0.12	0.53***	0.23*	0.54**	0.27***
	Large Protists	0.42***	-0.33***	0.54***	0.05	0.50***	0.31***
	Small Copepods	0.47***	-0.13	0.45***	0.43***	0.51***	0.48***
	Lg Copepods Day	-0.02	0.07	-0.04	-0.02	-0.03	-0.04
	Lg Copepods Night	NA: No night dives conducted this deployment					
Sep 2017	Fritillaria	0.44***	0.15***	0.46***	0.20***	0.45***	0.24***
	App. Others	0.28***	-0.24***	0.38***	0.00	0.31***	-0.05
	Large Protists	0.47***	0.00	0.51***	0.17***	0.50***	0.22***
	Small Copepods	0.71***	0.36***	0.74***	0.38***	0.73***	0.44***
	Lg Copepods Day	-0.03	0.01	-0.01	0.03	0.00	0.03
	Lg Copepods Night	0.08***	0.04	0.06***	0.04	0.09***	0.06
Nov-Dec 2017	Fritillaria	0.11***	0.00	0.08***	0.10**	0.03	0.15***
	App. Others	0.35***	-0.04	0.28***	0.57***	0.17***	0.69***
	Large Protists	0.46***	0.06	0.28***	0.33***	0.10***	0.46***
	Small Copepods	0.82***	0.67***	0.40***	0.33***	0.26***	0.51***
	Lg Copepods Day	0.15***	0.19**	0.04	0.23***	0.03	0.25***
	Lg Copepods Night	0.27***	0.18***	0.03*	0.27***	0.07***	0.21***
Jan-Feb 2018	Fritillaria	0.23***	-0.08	0.17***	0.06	0.20***	0.17***
	App. Others	0.68***	0.09	0.65***	0.12***	0.55***	0.07
	Large Protists	0.39***	-0.08	0.37***	0.10**	0.37***	0.27***
	Small Copepods	0.82***	0.22***	0.70***	0.26***	0.83***	0.73***
	Lg Copepods Day	0.22***	0.12	0.34***	0.29***	0.22***	0.14*
	Lg Copepods Night	0.54***	0.24***	0.60***	0.41***	0.50***	0.31***
Apr 2018	Fritillaria	0.58***	0.44***	0.43***	0.06	0.58***	0.12***
	App. Others	0.61***	0.02	0.44***	-0.04	0.60***	0.07*
	Large Protists	0.60***	0.26***	0.38***	-0.05	0.56***	0.09**
	Small Copepods	0.73***	0.50***	0.50***	-0.12***	0.71***	0.03
	Lg Copepods Day	0.20***	0.18***	0.15***	-0.00	0.19***	0.06
	Lg Copepods Night	0.27***	0.27***	0.21***	0.10*	0.30***	0.17***
Jul-Aug 2018	Fritillaria	0.23***	-0.08	0.15***	0.26***	0.05	0.05
	App. Others	0.61***	0.19**	0.46***	0.21***	0.55***	0.36***
	Large Protists	0.37***	-0.35***	0.34***	0.02	0.42***	0.06
	Small Copepods	0.70***	0.62***	0.40***	0.10	0.70***	0.55***
	Lg Copepods Day	0.07***	0.14	0.07***	0.07	0.08***	0.11
	Lg Copepods Night	0.26***	-0.04	0.25***	0.18	0.25***	0.26**
Oct 2018	Fritillaria	0.36***	0.21***	0.29***	0.16***	0.39***	0.23***
	App. Others	0.55***	-0.14***	0.39***	0.26***	0.50***	0.18***
	Large Protists	0.48***	0.12***	0.34***	0.27***	0.48***	0.36***
	Small Copepods	0.76***	0.35***	0.54***	0.38***	0.71***	0.52***
	Lg Copepods Day	0.00	0.12**	-0.00	0.10*	0.02	0.10*
	Lg Copepods Night	0.15***	0.04	0.10***	0.14***	0.13***	0.13**

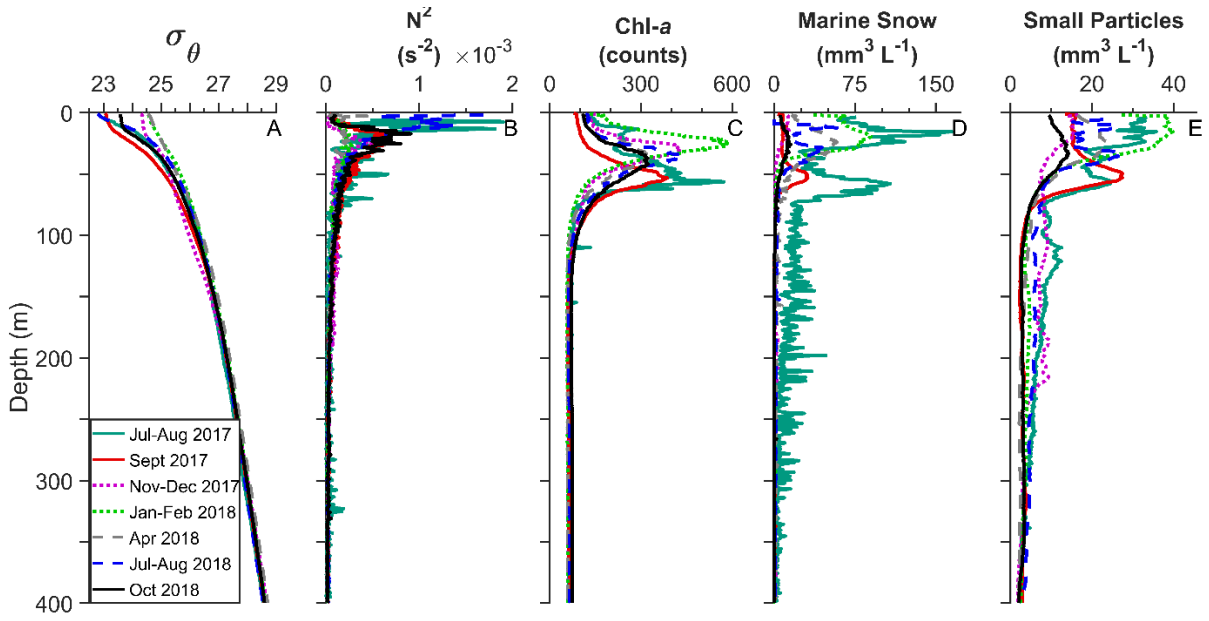

Supplementary Figure 1. Summary vertical profiles of water column properties and potential prey sources for all seven *Zooglider* deployments (0 - 400 m). (A) Potential density (σ_θ), (B) buoyancy frequency squared (N^2), (C) Chl-*a* fluorescence, (D) marine snow biovolume, and (E) small particle biovolume. Each vertical profile represents the mean of all dives (both day and night) within a deployment.

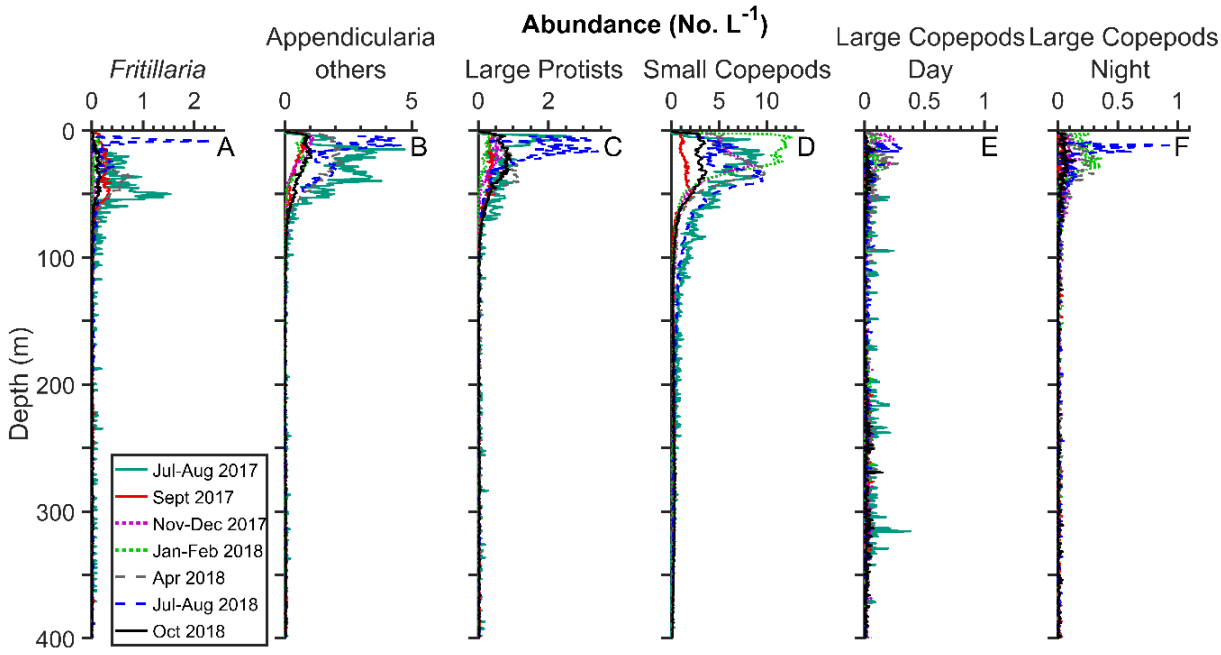

Supplementary Figure 2. Summary vertical profiles of mesozooplankton taxa for all seven *Zooglider* deployments (0 - 400 m). (A) *Fritillaria*, (B) other appendicularia, (C) large protists, (D) small copepods (feret diameter ≤ 3 mm), (E) large copepods (feret diameter > 3 mm) by day, (F) large copepods by night (all as No. L^{-1}). Each vertical profile represents the mean of all dives within a deployment.